Interkinetic nuclear movements promote apical expansion in pseudostratified epithelia at the expense of apicobasal elongation

Marina A. Ferreira[2,+], Evangeline Despin-Guitard[1], Fernando Duarte[1], Pierre Degond[2¶] and Eric Theveneau[1¶]

1. Centre for Developmental Biology, Centre for Integrative Biology, CNRS, Université Paul Sabatier, 118 route de Narbonne, 31062 Toulouse Cedex 09, France.

2. Department of Mathematics, Imperial College London, London, SW7 2AZ, United Kingdom.

+. Current address. University of Helsinki, Department of Mathematics and Statistics, P.O. Box 68, FI-00014 Helsingin yliopisto, Finland.

*corresponding authors: eric.theveneau@univ-tlse3.fr ; p.degond@imperial.ac.uk

Abstract

Pseudostratified epithelia (PSE) are a common type of columnar epithelia found in a wealth of embryonic and adult tissues such as ectodermal placodes, the trachea, the ureter, the gut and the neuroepithelium. PSE are characterized by the choreographed displacement of cells' nuclei along the apicobasal axis according to phases of their cell cycle. Such movements, called interkinetic movements (INM) have been proposed to influence tissue expansion and shape and suggested as culprit in several congenital diseases such as CAKUT and esophageal atresia. INM rely on cytoskeleton dynamics just as adhesion, contractility and mitosis do. Therefore, longer term impairment of INM without affecting proliferation and adhesion is currently technically unachievable. Here we bypassed this hurdle by generating a 2D agent-based model of a proliferating PSE and compared its output to the growth of the chick neuroepithelium to assess the interplay between INM and these other important cell processes during growth of a PSE. We found that INM directly generates apical expansion and apical nuclear crowding. In addition, our data strongly suggest that apicobasal elongation of cells is not an emerging property of a proliferative PSE but rather requires a specific elongation program. We then discuss how such program might functionally link INM, tissue growth and differentiation.

Authors Summary

Pseudostratified epithelia (PSE) are a common type of epithelia characterized by the choreographed displacement of cells' nuclei along the apicobasal axis during proliferation. These so-called interkinetic movements (INM) were proposed to influence tissue expansion and suggested as culprit in several congenital diseases. INM rely on cytoskeleton dynamics. Therefore, longer term impairment of INM without affecting proliferation and adhesion is currently technically unachievable. We bypassed this hurdle by generating a mathematical model of PSE and compared it to the growth of an epithelium of reference. Our data show that INM drive expansion of the apical domain of the epithelium and suggest that apicobasal elongation of cells is not an emerging property of a proliferative PSE but might rather requires a specific elongation program.

Introduction

Pseudostratified epithelia (PSE) are a special type of columnar epithelia in which cells are thin and elongated. Nuclei packing is very high and forces cells to distribute their nuclei along the apicobasal axis creating multiple layers of nuclei within a monolayer of cells, hence the term pseudostratification. PSE are found across the animal kingdom from invertebrates to vertebrates [1]. During development, several structures adopt a pseudostratified configuration such as the placodes and the central nervous system in vertebrates or the imaginal discs in Drosophila. In adults, PSE can be found along the respiratory, urinary and digestive tracts (e.g trachea, ureter, midgut) [2, 3] and various organs such as the gonads (e.g. epididymis) or the eye (lens, retina) [1]. One characteristic feature of PSE is the coordinated movements of nuclei during the cell cycle called interkinetic nuclear movements (INM) [4]. INM are decomposed in several steps: an apical to basal movement occurring during the G1 and S phases of the cell cycle and a basal to apical nuclear movement occurring during the G2 and M phases. The apical-ward movement, sometimes referred to as PRAM (Pre-mitotic Rapid Apical Movement), can be achieved via microtubules like in the chick neuroepithelium [5] or in the brain of mouse and rat embryos [6, 7] as well as in the retina of post-natal mice [8]. Such movements can also occur in an actomyosin-dependent manner as observed in the retina of fish embryos [9]. The return of nuclei to basal positions after mitoses was initially proposed to be passive and a direct consequence of nuclear crowding in the apical region of PSE. However, there are numerous evidence indicating an active role of the cytoskeleton in apical to basal nuclear displacement. For instance, Kif1A, an anterograde molecular motor of microtubules, is required for the apical to basal movement of nuclei in rat brain [7]. In addition, in mouse telencephalon, myosin II was shown to be essential for apical to basal movement [10]. Further, in ferrets’ brains apical to basal movements of nuclei are faster than basal to apical movements suggesting that the nuclear movement towards basal regions of the brain is active while the opposite is observed in mouse [11]. All these observations indicate that INM is regulated by cytoskeleton-dependent mechanisms and that the actual mechanism employed differs from species to species and organ to organ.

One consequence of the cytoskeleton-based regulation of INM is that it renders INM difficult to study in vivo since it is far from the only cell process that relies on cytoskeleton dynamics. Cell-cell, cell-matrix adhesions and cell contractility require normal microfilaments and microtubules dynamics and mitosis relies on microtubules-driven separation of chromosomes and actomyosin-dependent cytokinesis. Therefore, it is currently technically impossible to study the specific roles that INM might have in PSE dynamics, growth and shape over long periods of time (hours to days) without impairing adhesions, contractility or cell division. This motivates the use of alternative approaches, such as computational modelling.

Many models of cell tissue mechanics can be found in the literature, ranging from agent-based [12] to continuum models [13, 14]. Agent-based models describe the tissue at the cell scale and have been used to study local phenomena, such as the influence of the variation of spatial constraints in the cell cycle [15], how curvature of an epithelial sheet is determined by mechanical tensions [16] or how contact inhibition of locomotion generates forces in the tissue [17]. Continuum models instead describe the system at the tissue scale (cell density) and study global properties, such as the tissue curvature, resistance to deformation [18], contraction-elongation and tissue shear flow [13]. Despite being easier to treat, both computationally and analytically, continuum models do not incorporate all information about individual cell shape and position. An agent-based model instead is able to provide detailed spatial information and, in particular, it can account for variability in cell characteristics associated with the different stages of the cell cycle and variability in cell shape associated with the dynamics of INM (see [19] for a comparison between the continuum and agent-based frameworks). For these reasons, we opted for the agent-based approach. A large number of agent-based models of cell tissues have been developed in the last decades. The well-known Potts model [20] is a lattice-based model in which the cells may have complex shapes with a desired resolution. However, it has been reported that grid artefacts occur in cell movement and intercellular interactions [21] and they increase with particle density [22], which makes this model unsuited to describe crowded systems. Off-lattice models include for example the vertex model [15, 18, 23-25] and the Voronoi model [26, 27]. The tissue is regarded as a partition of space where each part represents one cell that is contiguous to its neighbours with no intercellular space between them. These models are able to describe densely packed systems. However, congestion is encoded into the model. In a PSE, nuclear crowding may not occur every time nor everywhere, so it should not be included in the model but rather occur as an emergent phenomenon.

Therefore, we reasoned that an appropriate framework to model a PSE would be an agent-based model where each cell moves in an off-lattice domain and interacts with its neighbours. Using such model, and comparing it with the chick neuroepithelium as a biological PSE of reference, we have explored the impact of INM, proliferation, adhesion and contractility on tissue shape, position of mitoses, pseudostratification and growth. Our results indicate that INM generates apical nuclear crowding, opposes apical shrinkage due to apical contractility and directly favors tissue growth oriented perpendicularly to the apicobasal axis (dorsoventrally, anteroposteriorly). Interestingly, all characteristics observed in the chick neuroepithelium such as apical positioning of mitoses, apical straightness, apical nuclear crowding and pseudostratification emerge from a combination of INM, proliferation, apical contractility and cell adhesion. However, the sustained linear apicobasal growth observed during development of the chick spinal cord cannot be reproduced with this combination of parameters. We show that neuroepithelial cells undergo a dramatic change of shape concomitantly to a reduction of cell volume while elongating along the apicobasal axis. This change of cell shape exceeds what is needed to accommodate new nuclei added by proliferation. Therefore, our simulations and in vivo observations strongly suggest that, while INM contributes to the expansion of the apical domain, the observed in vivo apicobasal elongation requires a specific elongation program. We then discuss whether such program, together with INM promoting apical nuclear crowding, might be a way to coordinate tissue growth and differentiation.

Results

Evolution of the chick trunk neuroepithelium from two to four days of development

As a biological PSE of reference, we chose the trunk neuroepithelium of the chick embryo. The neuroepithelium is a well-described PSE and has the advantage of being easily accessible for observation and manipulation. We started by monitoring the evolution of the neuroepithelium at the level of the prospective forelimb (somites 15-20) between two and four days of development [28], corresponding to developmental stage HH13- (18 somites, 48h of incubation) to stage HH23 (96 hours of incubation) and performed transversal cryosections (Fig 1A-B). Importantly, we focused on the intermediate region (half way between the dorsal and ventral sides of the tissue) to avoid the effect of extensive neuronal delamination and differentiation occurring in the ventral region of the tissue at these stages. We then performed immunostaining for phospho-histone H3 to label cells in mitosis and counterstained for actin and DNA (Fig 1C-D). We found that the dorsoventral size of the neuroepithelium increases 2.45-fold over two days, going from an average of 133µm to 326µm (Fig 1E), while the apico-basal size of the tissue grows by 2.3-fold from 50µm to 115µm (Fig 1F). Over the same period, the antero-posterior distance from somite 15 caudalward increases 3.56-fold, going from 2.6 to 9.4mm (S1 Fig). This indicates that growth of the posterior neuroepithelium between 2 and 4 days of development is biased toward anteroposterior growth. The number of pseudolayers of nuclei from apical to basal increases by 2.5-fold (Fig 1G). Interestingly, the distribution of nuclei changes from a homogenous distribution along the apicobasal axis in 48h-old embryos (Fig 1H, light green curve) to an accumulation of nuclei in the apical region in 72 and 96h-old embryos (Fig 1H, dark green curves). Note that nuclei density is lower in the basal region of the epithelium (Fig 1D). A change of average nuclear shape is also observed. The aspect ratio goes from 1.67 at 2 days to 2.01 at 4 days (Fig 1I). Nuclei become more elongated along the apicobasal axis (Fig 1D). This is due to a shortening of the nuclear length along the DV axis between 2 and 3 days of development while the length along the AB axis remains constant. By contrast, other parameters such as the straightness of the apical domain (Fig 1J), or the mean position of mitoses along the apicobasal axis (Fig 1K-L) do not significantly change (fold change inferior to 1.1). From these observations, we next wondered whether the balance between cell adhesion, proliferation and INM would be sufficient to drive the growth of the neuroepithelium, the progressive apical accumulation of nuclei and the increased pseudostratification, while apical positioning of mitoses and apical straightness remain constant.

Fig 1. Growth of caudal neuroepithelium of the chicken embryo from 2 to 4 days of development. A. Diagram of a chicken embryo at 48h of incubation (stage HH13-, 18 somites). B, transversal cryosections at the level of the forelimb at 48h, 72 and 96h of incubation. C-D, Confocal images of the intermediate region of the neuroepithelium at the level of the forelimb at 48, 72 and 96h of incubation, nuclei are stained with DAPI (grey) and actin with Phalloidin (green). Magenta line, apical domain; cyan line, basal domain. Note that the basal region progressively becomes devoid of nuclei. E, net dorsoventral length of the neural tube. F, net apicobasal length of the neural tube. G, number of pseudolayers of nuclei along the apicobasal axis. H, distribution of DAPI intensity along the apicobasal axis, normalized to the peak intensity in each dataset and to the apicobasal size so that the various stages can be compared. I, ratio of apicobasal and dorsoventral length of nuclei. J, straightness of apical domain (net distance between dorsal-most and ventral-most points of the apical surface divided by the actual length of the apical surface between these two points). K, positions of mitotic cells (either phospho-histone H3-positive cells or cells with condensed chromosomes from DAPI staining), at scale with the actual apicobasal size of the neural tube. L, positions of mitoses, raw data. Descriptive data collected from 20 embryos. Dots represent mean values. Error bars show the standard deviation. Box and whiskers plot: the box extends from the 25th to the 75th percentile; the whiskers show the extent of the whole dataset. The median is plotted as a line inside the box. AB, apicobasal; DV, dorsoventral; HH, Hamburger-Hamilton stages of chicken development; ss, somites.

Agent-based model of PSE dynamics

To be able to assess the impact of INM versus other cytoskeleton-dependent processes (e.g. adhesion, mitosis), we built an agent-based model of the neuroepithelium.

The chick neuroepithelium is an elongated PSE meaning that cells are very thin tubes with a large protruding nucleus giving them a watermelon-in-a-sock morphology (Fig 2A, S1 Movie). Cells are polarized according to the apicobasal axis with most of the cell-cell junctions localized apically and, conversely, the cell-matrix adhesions located basally [29]. In the model, each cell is approximated to a nucleus, an apical point and a basal point. The two points are attached to the nucleus via dynamic adjustable springs representing the viscoelastic properties of the cytoplasm (Fig 2B). Cells are placed next to one another along a lateral axis perpendicular to the apicobasal axis. Since the model is in 2D, this lateral axis can represent either the dorsoventral axis or the anteroposterior axis. Importantly, cells cannot intercalate nor swap positions. To model cell-cell and cell-matrix interactions we use simple mechanical and behavioural rules. On the apical side, apical points are attached to each other by apical-apical springs representing cell-cell adhesion. On the basal side, basal points are attached to a fixed basal line representing the basal lamina of the epithelium. Basal points can only move along the basal line and a maximum distance between adjacent basal points is implemented to avoid uncontrolled flattening of the tissue along the basal line. As in the real epithelium, apical points are only attached to their direct neighbors and thus can move within the 2D domain. Neuroepithelial cells are known to keep a straight shape. Thus, an alignment mechanism is set to prevent the apical point, the nucleus and the basal point of each cell from deviating significantly from a straight line. Nuclei cannot overlap. In the literature, non-overlapping constraints are approximated by a soft repulsion potential [30]. However, despite being computationally less expensive, this approximation becomes less and less accurate as the compression forces generated by congestion increase. Instead, we consider the nucleus being formed by an inner sphere (the hard core) and an outer sphere (the soft core). This representation allows soft cores to overlap with one another representing the deformation that would occur when two nuclei are pressed against each other [31]. In the chick neuroepithelium, nuclei are slightly compressed along the dorsoventral axis, giving them an elongated form along the apicobasal axis (see Fig 1C-D). Overlap of soft cores leads to a repulsive force which is controlled by the non-overlapping constraints imposed to the nucleus inner core.

Fig 2. Agent-based model of the pseudostratified epithelium. A. 3D confocal image of a single neuroepithelial cells expressing membrane-GFP, in a 2-day old chick neuroepithelium (see S1 Movie). B. Cells in the model are abstracted to a nucleus attached to a set of springs. C, implementation of cell cycle and INM during the simulation. Cells in the model constantly proliferate by going through a simplified cell cycle corresponding to three phases: a G1/S/passive G2 phase during which springs connected to the nucleus adjust to local constraints, a PRAM/active G2 phase during which apical-nucleus springs shrink while nucleus-basal springs elongate to recapitulate INM movements and the M phase during which springs behave as in G2. In addition, the hard core of nuclei enlarges in M phase to account for cell swelling and stiffening. Finally, at the end of the M phase each cell gives two daughter cells. One is systematically kept within the 2D-plane, the other daughter cell can be excluded. This parameter allows to control the rate of growth of the tissue independently of the pace of the cell cycle. See Supplementary Information for a detailed description of the model.

A clock, representing a simplified cell cycle, rules the proliferation rate. This *in silico* cycle has 3 phases. A first phase corresponding to G1, S and the part of G2 during which no directed movements of nuclei take place (Fig 2C; G1/S/passive G2). A second phase accounting for the active nuclear movements occurring in G2 known as pre-mitotic rapid apical movements (PRAM; Fig 2C, PRAM/active G2). A third phase representing Mitosis (Fig 2C; M). PRAM are implemented as follows: in cells entering active G2, the preferred rest length of apical-nucleus springs is set to 0 and the preferred rest length of the nucleus-basal spring is set to the current height of the cell. This drives an active apical-ward movement of the nuclei. In addition, during mitosis, the hard core of the nucleus increases (Fig 2C). Given that in our model cells have no cytoplasm, the increase of the hard core represents the known swelling and stiffening of cells during mitoses [32, 33]. At the end of mitosis daughter cells can be kept within the 2D-plane of the model or excluded. Thus, by systematically excluding 50% of the daughter cells we can keep the size of the cell population constant. This allows us to decouple the cell cycle and INM from actual proliferation (increase of cell number over time). Importantly, given the current lack of consensus about systematic active basal-ward movement of nuclei during G1 and S phases, we chose not to implement active movements of nuclei toward the basal side of the tissue in our model.

Outside of the PRAM/active G2 and M phases, apical-nucleus and nucleus-basal springs adjust their preferred rest length to their actual length, thus incorporating viscous behavior into the cytoplasm dynamics. This allows cells to accommodate their nuclei all along the apicobasal axis according to local constraints and forces (e.g., the position of the other nuclei or the forces on the various springs). Furthermore, there is a noise factor that allows nuclei to randomly move from their current location at each iteration of the simulation. In the chick neuroepithelium, nuclei are not known to display large scale random movements outside of PRAM. Thus, in our simulations, the noise is set very low compared to PRAM.

Each simulation is initialized with 30 cells. All cells have their apical point, nucleus and basal point aligned. Apical points and basal points are evenly distributed. This can be seen in the first frame of S2, S3 and S4 Movies. Then, at each time-iteration, the simulation runs as follows: springs and nuclei are updated according to the position of each cell in the cell cycle, cells that are in mitosis divide and noise is implemented. Mitosis and noise may lead to the violation of the non-overlapping constraints on the nuclei hard cores. A minimization algorithm developed in [34] is then used to obtain an admissible configuration. This configuration corresponds to a local minimizer of the total mechanical energy in the system associated to the springs, nuclei soft core and alignment forces. A complete description of the mathematical model can be found in Supplementary Information and all parameters used for the simulations presented in all figures hereafter are summarized in S1 Table.

INM opposes apicobasal elongation, generates apical nuclear crowding and enlarges the apical domain

To start with, we checked the evolution of the tissue in absence of proliferation (no INM, Fig 3) to assess the influence of cell-cell, cell-matrix adhesions and the non-overlapping constraints between nuclei. To do so, we set the minimum duration of the cell cycle to 10000 hours making it unlikely that any cells would divide during the course of the 48-hour simulation. The apical-apical springs were set to be passive, meaning that they do not adjust their size in response to stretch or compression. In these conditions, there is no change in apicobasal size of the tissue (Fig 3A, red curve, AB) with nuclei distributing homogenously halfway along the apicobasal axis (Fig 3A, red curve, N). The number of pseudolayers remains constant (Fig 3B, red curve) and the apical domain stays flat (Fig 3C, red curve). See S2 Movie. In order to assess the effect of INM without adding more cells to the tissue, we set the exclusion rate of daughter cells to 50%. This means that after mitosis only one of the daughter cells was kept in the 2D-plane, keeping the total cell number constant. The total cell cycle duration is set to a range of 10 to 21 hours corresponding to averages of the known values for the duration of the cell cycle in the chick trunk neuroepithelium between 2 and 4 days of development [35]. G2 and M phases respectively last 90 and 30 minutes each, however active nuclear movements corresponding to PRAM only occur in a fraction of the total G2. Thus, in the model to generate normal INM conditions we set PRAM/active G2 and M phases to 30 min each (normal INM, Fig 3A-C, black curves). To generate low INM conditions where cells actively displace their nuclei for a shorter period, we set the duration of PRAM/active G2 to 0 and M to 6 minutes (one iteration only) (low INM, Fig 3A-C, brown curves). Introducing low or normal INM slightly reduces the apicobasal size of the tissue (Fig 3A, brown and black curves AB are below the corresponding red curve) and the average position of nuclei shifted apically (Fig 3A, brown and black curves N are above the corresponding red curve). Adding INM also leads to a slight decrease in terms of pseudolayers (Fig 3B, black curve) and apical straightness (Fig 3C, black curve). Normal INM parameters lead to apical mitosis whereas low INM lead to a widespread distribution of mitoses along the apicobasal axis (Fig 3D). These data indicate that INM is sufficient to drive global nuclear apical crowding (Fig 3A, black curve), to slightly destabilize apical straightness and of course to control apical positioning of mitoses. In addition, we checked the lateral expansion of the apical, nuclear and basal domains under each of these 3 conditions. Each domain is defined by the length between the proximal and distal apical, nuclear and basal points along the lateral axis, respectively (Fig 3E-G). These analyses reveal that INM promotes the expansion of the apical domain, especially when all mitoses are apical (Fig 3E-G, magenta curves, arrow). See S2 Movie.

Fig 3. INM opposes apicobasal elongation, generates apical nuclear crowding and enlarges the apical domain. Simulations with passive apical-apical springs with INM (black and brown curves) or without INM (red curves) with constant cell number (see S2 Movie). A, Apicobasal length of the PSE (AB) and mean nuclear position along the AB axis, expressed in micrometers. Note that INM reduces apicobasal length (black curve with open circles (INM) is below the red curve (no INM)) and generates apical nuclear crowding (black curve with closed circles (INM) is above the red curve (no INM)). B, Number of layers of nuclei along the AB axis. C, straightness of apical domain (net distance between the first and last apical point divided by the actual distance between these two points). D, Position of mitoses along AB axis, 1 being apical. E-F, mean width of apical (magenta), nuclear (black) and basal (cyan) domains of the PSE over time. For each domain, the distance the between the first and last point along the lateral axis is computed and its evolution plotted over time. Note that INM promotes enlargement of the apical domain (panel 3G, arrow). Each simulation was performed over 480 iterations (48h of biological time) for 10 repetitions. Each curve represents the mean value of each dataset for the parameter plotted. Box and whiskers plot: the box extends from the 25th to the 75th percentile; the whiskers show the extent of the whole dataset. The median is plotted as a line inside the box.

Apical domains of epithelia are known to be dynamic and to display actomyosin contractility [36]. In addition, epithelial cells are known to resolve local imbalances in tension, compression and shear by aligning their cytoskeleton [37]. Further, apical constriction is known to be important for epithelial cell shape changes from squamous to columnar which corresponds to an apicobasal elongation [16, 36]. Thus apical constriction may be an important driving force for apicobasal elongation in PSE. To explore this hypothesis, we first check that actomyosin contractility was important in the chick neuroepithelium by treating samples with the ROCK inhibitor, a compound specifically blocking Rho-dependent myosin contractility (S2 Fig). Indeed, a brief 2-hour treatment with the ROCK inhibitor leads to a decrease of the apicobasal length, a reduction in pseudostratification, a rounding of nuclei and a decrease of the apical straightness. In addition, mitoses are not systematically apical (S2 Fig). These data indicate that the chick neuroepithelium has a short-term reliance on actomyosin contractility to maintain its shape and mitoses positions. Therefore, we ran the same simulations as above but setting the preferred rest length of apical springs to 0 in order to model overall apical contractility. Therefore, apical springs dynamically adjust their sizes to reach this rest length (Fig 4). We found that introducing contractile apical springs leads to a slight increase of apicobasal elongation (Fig 4A, AB curves) but overall nuclear positioning (Fig 4A, N curves), pseudostratification (Fig 4B) and tissue shape (Fig 4C) are not dramatically affected by having a contractile apical domain. In the absence of INM, contractile apical springs lead to a rapid shrinkage of the apical domain (Fig 4E, arrowhead). This effect is prevented by adding INM (Fig 4G, arrow) indicating that apical mitoses can oppose apical constriction (S2 Movie).

Fig 4. INM opposes apical constriction. Same simulations as in Fig 3 but with contractile apical-apical springs with INM (black and brown curves) or without INM (red curve), with constant cell number (see S2 Movie). A, Apicobasal length of the PSE (AB) and mean nuclear position along the AB axis, expressed in micrometers. B, Number of layers of nuclei along the AB axis. C, straightness of apical domain (net distance between the first and last apical point divided by the actual distance between these two points). D, Position of mitoses along AB axis, 1 being apical. E-G, mean width of apical (magenta), nuclear (black) and basal (cyan) domains of the PSE over time. For each domain, the distance the between the first and last point along the lateral axis is computed and its evolution plotted over time. Note that apical contractility reduces the width of the apical domain (panel 4E, arrow), whereas introducing INM opposes apical constriction (panel 4G, arrow; red curve in G is higher than in E). Each simulation was performed over 480 iterations (48h of biological time) for 10 repetitions. Each curve represents the mean value of each dataset for the parameter plotted. Box and whiskers plot: the box extends from the 25th to the 75th percentile; the whiskers show the extent of the whole dataset. The median is plotted as a line inside the box.

Increase in cell number strongly increases pseudostratification but has a weak effect on apicobasal elongation

Since neither INM nor apical constriction are sufficient to drive extensive apicobasal elongation, we next wanted to compare the impact of having passive or contractile apical-apical springs in the context of increasing cell number by proliferation (allowing more than one daughter cell to remain in the 2D plane after mitosis). For that, we ran two sets of simulations with passive or contractile apical-apical springs and with different rates of exclusion of daughter cells ranging from 0% (all cells generated by mitosis are added to the 2D plane) to 50% (one daughter cell is systematically excluded). INM is set to normal with PRAM/active G2 and M phases lasting 30 min each in all conditions. All outputs of simulations with passive apical-apical springs are plotted in shades of grey to black whereas outputs for simulations with contractile apical-apical springs are plotted in shades of hot colors from yellow to dark red. Contractile apical-apical springs have a slight positive impact on tissue apicobasal elongation (Fig 5A, AB curves; all colored curves are above their corresponding grey-to-black curves). This is accompanied by a slight apical shift of nuclei (Fig 5A, N curves). Pseudostratification correlates directly with the number of cells retained in the 2D plane (Fig 5B). At maximal (50%) or intermediate (40%, 30%) exclusion rates of daughter cells, contractile apical-apical springs further increase pseudostratification (Fig 5B, orange and red curves are above their cognate grey-to-black curves; S3 Movie). This effect is lost when all cells are retained (Fig 5B, 0% exclusion, yellow and grey curves overlap). With passive apical-apical springs the PSE shape becomes very sensitive to an increase of cell number. The more cells are kept within the 2D plane of the epithelium the faster apical straightness decreases (Fig 5C). Introducing contractile apical-apical springs mitigates the effect of hyper-proliferation (Fig 5C, orange and red curves stay close to straightness of 0.9). We then monitored the lateral expansion of apical, nuclear and basal domains over time for all conditions (Fig 5D-I). Increase in cell number induces a rapid expansion of the apical domain (Fig 5D-F). Interestingly, the apical shrinkage induced by contractile apical springs (Fig 5G, red curve) can be opposed by increasing the number of cells (Fig 5H-I, magenta curves). In addition, apical contractility positively feeds back into basal expansion. Note that the cyan curves in panels 5H and 5I increase faster than in panels 5E and 5F. These data indicate that an increase in total cell number drives a slight increase in apicobasal length, strongly drives pseudostratification and, in addition to INM, leads to an expansion of the apical domain. Interestingly, in the context of increasing cell number, apical contractility promotes basal rearrangements, an effect not seen with constant cell numbers (compare the cyan curves in panels 3E-G and 4E-G, with cyan curves in panel 5D, 5G). Further, apicobasal constriction slightly contributes to pseudostratification and helps maintain tissue shape during tissue growth.

Fig 5. Increase in cell number drives pseudostratification and apical contractility feeds back into basal rearrangements. Simulations with passive or contractile apical springs, normal INM and various rates of exclusion of daughter cells (see S3 Movie). A, apicobasal length of the PSE

(AB) and mean nuclear position along the AB axis (N) over time expressed in micrometers. B, Number of pseudolayers of nuclei along the AB axis. C, straightness of apical domain (net distance between the first and last apical point divided by the actual distance between these two points). D-F, mean width of apical (magenta), nuclear (black) and basal (cyan) domains of the PSE with passive apical-apical springs over time with 50 (D), 40 (E) and 30% (F) of daughter cells being excluded from the 2D plane. G-I, mean width of apical (magenta), nuclear (black) and basal (cyan) domains of the PSE with contractile apical-apical springs over time with 50 (G), 40 (H) and 30% (I) of daughter cells being excluded from the 2D plane. For each domain, the distance the between the first and last point along the lateral axis is computed and its evolution plotted over time. Note that apical contractility leads to basal rearrangements (compare cyan curves in H-I grow faster than in E-F). Each simulation was performed over 480 iterations (48h of biological time) for 10 repetitions. Each curve represents the mean value of each dataset for the parameter plotted.

Neuroepithelial cells undergo a dramatic change in shape that exceeds what is needed to accommodate nuclei along the apicobasal axis

So far, our simulations reveal that a progressive increase of pseudostratification, apical nuclear accumulation and apical mitoses can emerge from cell-cell/cell-matrix adhesion, proliferation and INM. However, none of the conditions tested allows a rapid apicobasal elongation of the tissue over 48h. This suggests that something is missing in our model. To achieve fast apicobasal elongation, cells could either get bigger (increase of cell volume) or elongate beyond what is necessary to accommodate the increase in number of nuclei due to proliferation. Our descriptive in vivo data (Fig 1A-B) show that a region of low nuclei density is formed in the basal domain of the chick neuroepithelium between 48h to 96 hours of incubation. This is driven by INM in our model (Fig 3A). Such low basal density of nuclei has been seen in other elongated PSE as well [29]. This observation suggests that apicobasal elongation of cells may not be driven by the pilling of nuclei along the apicobasal axis. Could elongation be caused by a change of cell shape or are cells also changing in size? To answer this question, we dissected explants of the neuroepithelium from the forelimb region (facing somites 15 to 20) in embryos at 2, 3 and 4 days of development (Fig 6A). Neural tubes were enzymatically isolated from surrounding tissues and dissociated to produce a suspension of single neuroepithelial cells (see material and methods). Cells were automatically counted and their diameters retrieved using a cell counter. From these measurements, volumes were calculated. This analysis reveals that the mean volume of neuroepithelial cells decreases between 2 and 3 days of development and remains stable from 3 to 4 days (Fig 6B-C). We next checked the size of the apical domains by performing *en face* microscopy on neuroepithelia from the same stages (Fig 6A, D-E). We found that the mean area occupied by the cells' apical sides is also significantly getting smaller between 2 and 3 days of development but does not significantly change from 3 to 4 days (Fig 6D-E). These data indicate that neuroepithelial cells undergo a dramatic change of cell shape, together with a reduction of cell volume, which appear to exceed what would be needed to accommodate the increase of cell nuclei along the apicobasal axis. This strongly suggests that undifferentiated PSE cells specifically elongate rather than simply adjust to local nuclear crowding.

Fig 6. Mean volume and mean apical surface of chick neuroepithelial cells decreases between 2 and 3 days of development. A, Diagram depicting the regions used for the preparation of cell suspensions and open book histology from chicken embryos at 2, 3 and 4 days of development (see Methods for details of the experimental procedures). Region monitored (from somite 15 to 20, forelimb region) is indicated by a dotted line. B, representative images of neuroepithelial cells in suspension after neural tube dissection and enzymatic dissociation. C, mean volume of neuroepithelial cells over time (n_{48h}=82; n_{72h}=568; n_{96h}=1168). Cells get significantly smaller from 2 to 3 days of development and remain stable. Box and whiskers plot: the box extends from the 25th to the 75th percentile; the whiskers show the extent of the whole dataset. The median is plotted as a line inside the box. One-way ANOVA (Kruskal-Wallis) followed by Dunn's multiple comparisons. ****, $p<0.0001$; ns, $p>0.9999$. D, *en face* view of the apical domain of the intermediate region of the neuroepithelium (actin is stained by Phalloidin). E, mean area of the individual apical surfaces over time (n_{48h}=67; n_{72h}=66; n_{96h}=81). Apical surfaces shrink from 2 to 3 days of development and remain stable. Dots represent mean of the dataset, error bars represent S.D. One-way ANOVA followed by multiple comparisons. ****, $p<0.0001$; ns, $p=0.1586$.

Apicobasal elongation requires a specific elongation force

Therefore, we wondered whether adding a global non-oriented expansion force might account for the apicobasal elongation observed in vivo. To do that, we increased the amount of noise on nuclear position at each iteration. All nuclei are allowed to move in a random direction at each iteration of the simulation. Since apical-nucleus and nucleus-basal springs are able to update their rest length to adjust to their actual size, any increase in random nuclear movements forces the apical-nucleus and nucleus-basal springs to stretch. Given that cells are attached to the basal line, to each other and that cells are prevented from bending due to an imposed alignment force, increasing random nuclear noise should generate a linear apicobasal elongation force. We ran simulations with conditions similar to those presented in

Fig 4 but with a 25-fold increase of random nuclear movements (Fig 7). Under these conditions, we observed a 2-fold increase in apicobasal length (Fig 7A, S4 Movie) whereas the number of pseudolayers (Fig 7B) and apical straightness (Fig 7C) were similar to the values obtained with low noise (Fig 5B-C). In addition, increasing noise does not affect the overall dynamics of lateral expansion of the tissue (Fig 7D-F). At low percentages of exclusion of daughter cells (30%) the lateral expansion of the apical domain is faster than that of the basal domain (Fig 7F, compare magenta and cyan curves). Thus, we attempted to solve this issue by allowing basal points to update their positions at a faster rate. This was sufficient to allow an isotropic expansion of the tissue (Fig 7G, black, cyan and magenta curves grow at the same pace; S4 Movie). Finally, our previous simulations (Figs 3 and 4) hinted that INM was capable of opposing apicobasal elongation. We wanted to check if this was still true under the extensive apicobasal growth generated by increased noise. We repeated the same simulations as shown in Fig 7, excluding 50% of daughter cells to keep total cell number constant, but setting low INM conditions with PRAM/active G2 set to 0 and M to 6min. (S3 Fig). Under low INM conditions, the PSE elongates along the apicobasal axis faster than with normal INM and there is a shrinkage of the apical domain (S5 Movie) confirming our previous observations.

Fig 7. Apicobasal elongation requires a specific elongation force. Simulations with contractile apical springs, normal INM and high noise. A, apicobasal length of the PSE (AB) and mean nuclear position along the AB axis (N) over time expressed in micrometers (see S4 Movie). B, Number of pseudolayers of nuclei along the AB axis. C, straightness of apical domain (net distance between the first and last apical point divided by the actual distance between these two points). D-G, mean width of apical (magenta), nuclear (black) and basal (cyan) domains of the PSE with dynamic apical-apical springs over time with 50 (D), 40 (E) and 30% (F-G) of daughter cells being excluded from the 2D plane. For each domain, the distance the between the first and last point along the lateral axis is computed and its evolution plotted over time. D-F, slow update of basal point positions (as in all previous Figs). G, fast update of basal point positions (twice faster). Each simulation was performed over 480 iterations (48h of biological time) for 10 repetitions. Each curve represents the mean value of each dataset for the parameter plotted.

In conclusion, our data indicate that: i/ pseudostratification is mainly controlled by the increase of cell number, ii/ apical contractility is essential to maintain tissue shape in the context of a high proliferation rate, iii/ INM promotes the expansion of the apical domain, iv/ INM opposes pseudostratification, apical constriction and apicobasal elongation whereas it controls apical positioning of mitosis and apical nuclear crowding, v/ apicobasal elongation of cells is likely to be due to an active elongation program and not a mere consequence of increased nuclear density (Fig 8).

Fig 8. Interplay between INM, proliferation and cell adhesion in the context of a specific apicobasal elongation program are needed to recapitulate normal PSE dynamics. Green arrows indicate positive action, red arrows indicate negative/inhibitory action. Dotted line indicate weaker effect than plain lines. PRAM, pre-mitotic rapid apical migration; PRAR, post-mitotic rapid apical removal; INM, interkinetic nuclear movement.

Discussion

Our simulations clearly link INM to the rapid emergence of nuclear crowding in the apical domain and to the formation of a region of low nuclear density in the basal part of the PSE. Yet, in vivo, the low nuclear density observed in the basal domain of the chick trunk neuroepithelium (forelimb level) only emerges in 3-to-4-day old embryos. This could be due to a lack of INM at early stages of neural plate/tube development. This is unlikely since apical mitoses have been observed even at open neural plate stages in chick and mouse embryos [38, 39]. Alternatively, at early stages, there could be a counterbalancing post-mitotic rapid apical removal (PRAR, Fig 8) of nuclei as part of the INM, as suggested in rats and ferrets' brains [7, 11]. Such active basal-ward movement would prevent the early formation of a crowded apical domain and that of a relatively loose basal domain. Neuroepithelial cells always detach from the apical surface upon differentiation into neurons but they can also be induced to detach from the apical surface by a local increase of the apical density of nuclei [40, 41]. Thus, it may be important to delay apical nuclear crowding to prevent early delamination of undifferentiated neural progenitors from the apical domain. Therefore, one could propose that regulation of the intensity of INM might control the onset of neuron delamination in order to synchronize neuronal differentiation with the development of the spinal cord itself. The loose basal region may also be needed to accommodate the cell body of delaminating neurons which accumulate in the basal side of the epithelium. In addition, or alternatively, INM might control the onset of neuron delamination in order to synchronize neuronal differentiation with the development of adjacent structures awaiting innervation. For instance, it would be interesting to see if somites (or the myotome), which produce muscles to be innervated, interfere with the patterns of INM in the adjacent neural tube.

Apical constriction is known to be essential to promote the apicobasal elongation driving the switch from squamous to cuboidal epithelial sheets [36]. Yet, in our simulation apical constriction was a poor driver of apicobasal elongation. This is likely due to the fact that in elongated PSE the apical surface is small compared to the size of the basolateral membrane of cells. In the trunk of a 2-day old chicken embryo, the diameter of the apical surface is around 5 microns whereas cells are already 50 microns tall. Thus, any change of the apical size will only have a marginal effect on cell height. At early stages, during the folding of the neural plate, actomyosin contractility is important and Rho and myosin are detected in the apical region of most neuroepithelial cells [42]. It is proposed that apical constriction may drive cell shape changes contributing to neural plate bending. However, the region that undergoes the most dramatic change of shape, the medial hinge point located at the midline above the notochord, has little and only transient accumulation of Rho. In addition, in mice with targeted defects in cytoskeletal genes, neurulation of the caudal neural tube is rarely affected [43]. Following observations in chick [44] and mouse [38, 45] embryos, it was alternatively proposed, that the change in cell shape at the medial hinge point could be driven by local differences in INM in the neural plate, with cells above the notochord having longer S-phase. The nuclei would spend more time in the basal regions favoring an enlargement of the basal domain. This would let cells adopt a pyramidal shape promoting tissue folding. As for the effect of apical constriction, a longer S-phase is unlikely to generate any significant change in cell shape in elongated PSE since the width of the nucleus only represent a small fraction of the total cell height. It is interesting to note that while the intermediate region of the neuroepithelium exhibits a fast linear increase in apicobasal size from 2 to 4 days of development, the cells located in the floor plate of the neural tube do not change significantly in height during this period. If indeed their pyramidal shape is linked to a specific cell cycle with a long S-phase, this relationship can only be maintained if the cells do not elongate beyond a size that would mitigate the effect of the position of the nucleus.

Histological analyses in mice with CAKUT (congenital anomalies of the kidney and urinary tract) or EA/TEF (Esophageal atresia/tracheoesophageal fistula) [2, 3] show a correlation between tissue expansion defects and local lack of INM. The local loss of INM (basal mitoses) correlates with problems of convergence extension and defects in tissue separation which were proposed to be due to a loss of apicobasal polarity in these syndromes. Interestingly, INM is not a permanent feature of all PSE. In mouse, INM stops around E13 in the esophagus meaning that from this stage basal mitoses naturally occur in this tissue [2]. By contrast, by E14, INM and apical mitoses can still be observed in the brain, the trachea, the ureter and the intestine. As with the correlation between lack of expansion and lack of INM in the aforementioned syndromes, it was proposed that INM might be a driving force of tissue expansion, since the organs in which it persists expand at a faster rate than the overall growth of the embryo at these stages. Here we show that INM directly contributes to expansion of the apical domain and thus promotes growth in axes perpendicular to the apicobasal axis (DV, AP). In vivo, other mechanisms likely contribute to tissue expansion along the dorsoventral or anteroposterior axis. One possibility is cell intercalation. This has been observed during neurulation in mouse [38]. The dorsal regions of the neural plate grow faster than the ventral regions. This is due in part to a faster cell cycle but also to significant cell intercalation from ventral to dorsal.

Another mechanism that could contribute to tissue expansion in one direction is the orientation of mitotic spindles. It was observed in the chick neural tube that, at early stages (HH7 to HH12, corresponding to 24 to 44h of incubation), most mitoses (circa 55%) were oriented along the anteroposterior axis [39]. Such percentages would correspond to an exclusion rate of daughter cells of 27% in our simulation. Therefore, with such a biased orientation, proliferation would favor anteroposterior elongation of the neuroepithelium compared to expansion in apicobasal and dorsoventral orientations. In addition, in most PSE studied, the mean cell cycle length tends to change over time. It can get longer in the caudal neural tube [35] and in the brain [46] or shorter as in the ureteric epithelium [3] and the midgut [47]. Changes in cell cycle length will obviously change the rate at which a tissue increases in terms of cell number but will also affect the frequency of INM events. Given that apical localization of mitoses drives expansion of the apical domain by opposing apical constriction, such changes in cell cycle pace may also affect tissue shape. Indeed, in our simulations, imbalances in proliferation and apical contractility were sufficient to promote either bending or buckling of the apical surface (see S4 Movie). To maintain tissue shape and straightness of the apical domain, the rapid expansion of the apical domain needs to be compensated by an equivalent expansion if the basal domain or hindered by extensive apical constriction.

Further, defects in microtubule dynamics can lead to lissencephaly and microcephaly two common neurodevelopmental defects due to improper growth of the brain. This prompted some to suggest that impaired INM, a microtubule-dependent phenomenon, might contribute to these pathologies [48, 49]. However, all of these microtubule-related defects have also problems in neuronal migration, mitotic spindle positioning and proliferation making it difficult to identify the effects specifically due to a lack of INM.

Finally, our data indicate that apicobasal elongation is likely to require a specific cell elongation program. In the model, we generated the elongation force using an artificially increased nuclear noise. Given that, outside of PRAM, such large scale random nuclear movements were never observed in the chick neuroepithelium, it is very unlikely that in vivo apicobasal elongation comes from a progressive increase in random nuclear movements. Most likely, it comes from an extensive reorganization of the cytoskeleton. Experimentally disentangling the various putative cytoskeleton-related mechanisms involved in INM (PRAM or PRAR) and cell elongation will required the generation of new tools for the fine-tuning of actin/tubulin dynamics over long periods of time (hours to days) without affecting proliferation.

Materials and Methods

Chicken eggs

Fertilized chicken eggs were obtained from S.C.A.L (Société Commerciale Avicole du Languedoc) and incubated at 38°C until the desired stage [28].

Histology and staining of chicken embryo samples

Embryos were soaked in Phosphate Buffer 15% sucrose overnight at 4°C. Then, embryos were transferred for 2 hours in gelatin 7.5%/ sucrose 15%. Small weighing boats are used as molds. A small layer of gelatin/sucrose is deposited at the bottom and left to set. Embryos are then transferred on the gelatin layer using a 2.5mL plastic pipette. Each embryo is placed in a single drop and left to set. Once all drops are set, an excess of gelatin/sucrose solution is poured on to the weighing boat to fill it. Once again gelatin is left to set on the bench. After setting, the dish is placed at 4°C for 1 hour to harden the gelatin. Once ready, the block of gelatin containing the embryos is placed under a dissecting microscope and individual blocks are carved to position the embryos in the desired orientation for sectioning. Cryosections were performed using a Leica CM1950 cryostat. Sections were incubated in PBS1X at 42°C for 30 minutes to remove the gelatin, treated with PBS1X, 1% triton, 2% serum for permeabilization and blocking. Primary antibodies were diluted in PBS1X 2% newborn calf serum and applied overnight at 4°C under a coverslip. Secondary antibodies were diluted in PBS1X and applied for 2 hours at room temperature. Washes were done in PBS1X. Antibodies used: mouse anti-phospho-histone 3 (Cell Signaling, MA312B). Counterstaining for actin and DNA was done with Phalloidin (1/1000) and DAPI (1/1000).

Suspension of neuroepithelial cells

Samples of the whole trunk between somite 15 and 20 were taken from embryos at 2, 3 and 4 days of development. The explants were incubated in Dispase II (Stem Cell Technologies; #07923, at 1U/mL) at 37°C for 20 minutes to degrade collagens and fibronectin. Tissues were then separated using mounted needles. Neural tube explants were then incubated in a trypsin solution (ThermoFisher, 25300054

Concentration) to generate single cells. From neural tube explants from 3-day and 4-day old embryos, numerous cells (most likely neurons) did not adopt a round morphology after dissociation, instead they maintained an elongated fiber-like morphology and accumulated at the bottom of the tubes. They were not included in the supernatant used for cell diameter analysis.

Open book observation

Samples of the whole trunk between somite 15 and 20 were taken from embryos at 2, 3 and 4 days of development. The neural tube was open from its dorsal side using forceps. The tip of one forceps is inserted in the neural tube lumen and moved along the anteroposterior axis to open the whole explant. Explants are then squeezed in between two coverslips to maintain them open. Apical side is positioned face down on an inverted microscope for observation.

Imaging

Confocal images were taken on a Zeiss 710 confocal microscope. Whole mount images were acquired on a Leica MZ10F.

Statistics

Statistical analyses of in vivo data were performed with Prism 6 (GraphPad). Datasets were tested for Gaussian distribution. Student t-tests or ANOVA followed by multiple comparisons were used with the appropriate parameters depending on the Gaussian vs non-Gaussian characteristics of the data distribution. Significance threshold was set at $p<0.05$.

In silico simulations and associated plots

The code was written in Fortran90 in sequential mode and the simulations were performed on a DELL Precision T7810 with windows 8.1, 64 bits of RAM, with two CPU Intel Xeon E52637 3.8 GHZ processors. The computational time of each simulation of the tissue evolution for 48 hours (480 time iterations) ranges from 8 minutes with 30 cells and no proliferation to approximately 40 minutes with proliferation and the exclusion rate of daughter cells set to 0%. For each set of in silico conditions at least 10 repetitions were performed. Data were processed using MatLab R2017b. Plots: for simplicity, mean values of each parameter were plotted at each time-iteration over 40 iterations (4hours) and error bars were not displayed. An example of error bars representing standard deviation can be seen on S3 Fig. To help visualizing differences between each in silico conditions, min and max values of equivalent graphs across the various Figs were kept constant.

Acknowledgements

We thank Drs Sara Merino-Aceituno, Samuel Tozer, Bertrand Benazeraf, Fabienne Pituello, Ariane Trescases and Elisa Marti for critical reading of the manuscript.

Authors' contributions

ET and PD conceived the project. MF and PD made the computational model with inputs from ET. ET, EDG and FD generated the biological data. ET designed and performed in silico simulations. ET, MF and PD interpreted and organized the data. ET, MF and PD wrote the manuscript. All authors commented on the manuscript.

Funding

ET acknowledges support from the Fondation pour la Recherche Médicale (FRM AJE201224), the Region Midi-Pyrénées (13053025), Toulouse Cancer Santé (DynaMeca), the CNRS and Université Paul Sabatier (UMR5547). FD and EDG were supported by Toulouse Cancer Santé (DynaMeca). PD acknowledges support by the Engineering and Physical Sciences Research Council (EPSRC) under grants no. EP/M006883/1 and EP/N014529/1, by the Royal Society International Exchanges under grant no. IE160750, by the Royal Society and the Wolfson Foundation through a Royal Society Wolfson Research Merit Award no. WM130048 and by the National Science Foundation (NSF) under grant no. RNMS11-07444 (KI-Net). PD is on leave from CNRS, Institut de Mathématiques de Toulouse, France. MF acknowledges support by Imperial College, Department of Mathematics, through a Roth PhD studentship, by The Company of Biologists, Disease Models and Mechanisms, through a Travelling fellowship and by the AtMath Collaboration of the Faculty of Science of the University of Helsinki. MF short-term stays at CNRS and Université Paul Sabatier (UMR5547) were further supported by Toulouse Cancer Santé via the DynaMeca grant. The funders had no role in study design, data collection and analysis, decision to publish, or preparation of the manuscript.

Data Availability Statement

All relevant data are within the manuscript and its Supporting Information files.

Competing interests

The authors have declared that no competing interests exist.

Ethics statement

This research only used chicken embryos at early stages of development (before the 6th day). None of the procedures fall under legal requirements for animal use and can be performed by anyone without animal licence.

References

1. Norden C. Pseudostratified epithelia - cell biology, diversity and roles in organ formation at a glance. Journal of cell science. 2017;130(11):1859-63. doi: 10.1242/jcs.192997. PubMed PMID: 28455413.
2. Kaneda R, Saeki Y, Getachew D, Matsumoto A, Furuya M, Ogawa N, et al. Interkinetic nuclear migration in the tracheal and esophageal epithelia of the mouse embryo: Possible implications for tracheo-esophageal anomalies. Congenit Anom (Kyoto). 2018;58(2):62-70. doi: 10.1111/cga.12241. PubMed PMID: 28782137.
3. Motoya T, Ogawa N, Nitta T, Rafiq AM, Jahan E, Furuya M, et al. Interkinetic nuclear migration in the mouse embryonic ureteric epithelium: Possible implication for congenital anomalies of the kidney and urinary tract. Congenit Anom (Kyoto). 2016;56(3):127-34. doi: 10.1111/cga.12150. PubMed PMID: 26710751.
4. Spear PC, Erickson CA. Interkinetic nuclear migration: a mysterious process in search of a function. Development, growth & differentiation. 2012;54(3):306-16. doi: 10.1111/j.1440-169X.2012.01342.x. PubMed PMID: 22524603; PubMed Central PMCID: PMCPMC3357188.
5. Spear PC, Erickson CA. Apical movement during interkinetic nuclear migration is a two-step process. Developmental biology. 2012;370(1):33-41. doi: 10.1016/j.ydbio.2012.06.031. PubMed PMID: 22884563; PubMed Central PMCID: PMCPMC3935435.
6. Kosodo Y, Suetsugu T, Suda M, Mimori-Kiyosue Y, Toida K, Baba SA, et al. Regulation of interkinetic nuclear migration by cell cycle-coupled active and passive mechanisms in the developing brain. The EMBO journal. 2011;30(9):1690-704. doi: 10.1038/emboj.2011.81. PubMed PMID: 21441895; PubMed Central PMCID: PMCPMC3101991.
7. Tsai JW, Lian WN, Kemal S, Kriegstein AR, Vallee RB. Kinesin 3 and cytoplasmic dynein mediate interkinetic nuclear migration in neural stem cells. Nature neuroscience. 2010;13(12):1463-71. doi: 10.1038/nn.2665. PubMed PMID: 21037580; PubMed Central PMCID: PMCPMC3059207.
8. Yu J, Lei K, Zhou M, Craft CM, Xu G, Xu T, et al. KASH protein Syne-2/Nesprin-2 and SUN proteins SUN1/2 mediate nuclear migration during mammalian retinal development. Human molecular genetics. 2011;20(6):1061-73. doi: 10.1093/hmg/ddq549. PubMed PMID: 21177258; PubMed Central PMCID: PMCPMC3043658.
9. Norden C, Young S, Link BA, Harris WA. Actomyosin is the main driver of interkinetic nuclear migration in the retina. Cell. 2009;138(6):1195-208. doi: 10.1016/j.cell.2009.06.032. PubMed PMID: 19766571; PubMed Central PMCID: PMCPMC2791877.
10. Schenk J, Wilsch-Brauninger M, Calegari F, Huttner WB. Myosin II is required for interkinetic nuclear migration of neural progenitors. Proceedings of the National Academy of Sciences of the United States of America. 2009;106(38):16487-92. doi: 10.1073/pnas.0908928106. PubMed PMID: 19805325; PubMed Central PMCID: PMCPMC2752599.
11. Okamoto M, Shinoda T, Kawaue T, Nagasaka A, Miyata T. Ferret-mouse differences in interkinetic nuclear migration and cellular densification in the neocortical ventricular zone. Neuroscience research. 2014;86:88-95. doi: 10.1016/j.neures.2014.03.011. PubMed PMID: 24780233.
12. Osborne JM, Fletcher AG, Pitt-Francis JM, Maini PK, Gavaghan DJ. Comparing individual-based approaches to modelling the self-organization of multicellular tissues. PLoS

computational biology. 2017;13(2):e1005387. doi: 10.1371/journal.pcbi.1005387. PubMed PMID: 28192427; PubMed Central PMCID: PMCPMC5330541.

13. Ishihara S, Marcq P, Sugimura K. From cells to tissue: A continuum model of epithelial mechanics. Phys Rev E. 2017;96(2-1):022418. doi: 10.1103/PhysRevE.96.022418. PubMed PMID: 28950595.

14. Kopf MH, Pismen LM. A continuum model of epithelial spreading. Soft matter. 2013;9(14):3727-34. doi: 10.1039/c3sm26955h. PubMed PMID: WOS:000316118300005.

15. Streichan SJ, Hoerner CR, Schneidt T, Holzer D, Hufnagel L. Spatial constraints control cell proliferation in tissues. Proceedings of the National Academy of Sciences of the United States of America. 2014;111(15):5586-91. doi: 10.1073/pnas.1323016111. PubMed PMID: 24706777; PubMed Central PMCID: PMCPMC3992650.

16. Hannezo E, Prost J, Joanny JF. Theory of epithelial sheet morphology in three dimensions. Proceedings of the National Academy of Sciences of the United States of America. 2014;111(1):27-32. doi: 10.1073/pnas.1312076111. PubMed PMID: 24367079; PubMed Central PMCID: PMCPMC3890844.

17. Zimmermann J, Camley BA, Rappel WJ, Levine H. Contact inhibition of locomotion determines cell-cell and cell-substrate forces in tissues. Proceedings of the National Academy of Sciences of the United States of America. 2016;113(10):2660-5. doi: 10.1073/pnas.1522330113. PubMed PMID: 26903658; PubMed Central PMCID: PMCPMC4791011.

18. Alt S, Ganguly P, Salbreux G. Vertex models: from cell mechanics to tissue morphogenesis. Philosophical transactions of the Royal Society of London Series B, Biological sciences. 2017;372(1720). doi: 10.1098/rstb.2015.0520. PubMed PMID: 28348254; PubMed Central PMCID: PMCPMC5379026.

19. Byrne H, Drasdo D. Individual-based and continuum models of growing cell populations: a comparison. Journal of mathematical biology. 2009;58(4-5):657-87. doi: 10.1007/s00285-008-0212-0. PubMed PMID: 18841363.

20. Scianna M, Preziosi L, Wolf K. A Cellular Potts Model simulating cell migration on and in matrix environments. Math Biosci Eng. 2013;10(1):235-61. doi: 10.3934/mbe.2013.10.235. PubMed PMID: 23311371.

21. Plank MJ, Simpson MJ. Models of collective cell behaviour with crowding effects: comparing lattice-based and lattice-free approaches. Journal of the Royal Society, Interface / the Royal Society. 2012;9(76):2983-96. doi: 10.1098/rsif.2012.0319. PubMed PMID: 22696488; PubMed Central PMCID: PMCPMC3479911.

22. Meinecke L, Eriksson M. Excluded volume effects in on- and off-lattice reaction-diffusion models. Iet Syst Biol. 2017;11(2):55-64. doi: 10.1049/iet-syb.2016.0021. PubMed PMID: WOS:000398811200001.

23. Farhadifar R, Roper JC, Aigouy B, Eaton S, Julicher F. The influence of cell mechanics, cell-cell interactions, and proliferation on epithelial packing. Current biology : CB. 2007;17(24):2095-104. doi: 10.1016/j.cub.2007.11.049. PubMed PMID: 18082406.

24. Fletcher AG, Osterfield M, Baker RE, Shvartsman SY. Vertex models of epithelial morphogenesis. Biophysical journal. 2014;106(11):2291-304. doi: 10.1016/j.bpj.2013.11.4498. PubMed PMID: 24896108; PubMed Central PMCID: PMCPMC4052277.

25. Staple DB, Farhadifar R, Roper JC, Aigouy B, Eaton S, Julicher F. Mechanics and remodelling of cell packings in epithelia. Eur Phys J E Soft Matter. 2010;33(2):117-27. doi: 10.1140/epje/i2010-10677-0. PubMed PMID: 21082210.

26. Bock M, Tyagi AK, Kreft JU, Alt W. Generalized Voronoi Tessellation as a Model of Two-dimensional Cell Tissue Dynamics. Bulletin of mathematical biology. 2010;72(7):1696-731. doi: 10.1007/s11538-009-9498-3. PubMed PMID: WOS:000282427900003.
27. Meineke FA, Potten CS, Loeffler M. Cell migration and organization in the intestinal crypt using a lattice-free model. Cell proliferation. 2001;34(4):253-66. doi: DOI 10.1046/j.0960-7722.2001.00216.x. PubMed PMID: WOS:000170564500006.
28. Hamburger V, Hamilton HL. A series of normal stages in the development of the chick embryo. 1951. Developmental dynamics : an official publication of the American Association of Anatomists. 1992;195(4):231-72. doi: 10.1002/aja.1001950404. PubMed PMID: 1304821.
29. Strzyz PJ, Matejcic M, Norden C. Heterogeneity, Cell Biology and Tissue Mechanics of Pseudostratified Epithelia: Coordination of Cell Divisions and Growth in Tightly Packed Tissues. Int Rev Cell Mol Biol. 2016;325:89-118. doi: 10.1016/bs.ircmb.2016.02.004. PubMed PMID: 27241219.
30. Van Liedekerke P, Palm MM, Jagiella N, Drasdo D. Simulating tissue mechanics with agent-based models: concepts, perspectives and some novel results. Comput Part Mech. 2015;2(4):401-44. doi: 10.1007/s40571-015-0082-3. PubMed PMID: WOS:000417453500008.
31. Pfisterer K, Jayo A, Parsons M. Control of nuclear organization by F-actin binding proteins. Nucleus. 2017;8(2):126-33. doi: 10.1080/19491034.2016.1267093. PubMed PMID: 28060557; PubMed Central PMCID: PMCPMC5403142.
32. Zlotek-Zlotkiewicz E, Monnier S, Cappello G, Le Berre M, Piel M. Optical volume and mass measurements show that mammalian cells swell during mitosis. The Journal of cell biology. 2015;211(4):765-74. doi: 10.1083/jcb.201505056. PubMed PMID: 26598614; PubMed Central PMCID: PMCPMC4657168.
33. Son S, Kang JH, Oh S, Kirschner MW, Mitchison TJ, Manalis S. Resonant microchannel volume and mass measurements show that suspended cells swell during mitosis. The Journal of cell biology. 2015;211(4):757-63. doi: 10.1083/jcb.201505058. PubMed PMID: 26598613; PubMed Central PMCID: PMCPMC4657169.
34. Degond P, Ferreira MA, Motsch S. Damped Arrow-Hurwicz algorithm for sphere packing. J Comput Phys. 2017;332:47-65. doi: 10.1016/j.jcp.2016.11.047. PubMed PMID: WOS:000393250800003.
35. Molina A, Pituello F. Playing with the cell cycle to build the spinal cord. Developmental biology. 2017;432(1):14-23. doi: 10.1016/j.ydbio.2016.12.022. PubMed PMID: 28034699.
36. St Johnston D, Sanson B. Epithelial polarity and morphogenesis. Current opinion in cell biology. 2011;23(5):540-6. doi: 10.1016/j.ceb.2011.07.005. PubMed PMID: 21807488.
37. Ladoux B, Mege RM, Trepat X. Front-Rear Polarization by Mechanical Cues: From Single Cells to Tissues. Trends in cell biology. 2016;26(6):420-33. doi: 10.1016/j.tcb.2016.02.002. PubMed PMID: 26920934; PubMed Central PMCID: PMCPMC5421599.
38. McShane SG, Mole MA, Savery D, Greene ND, Tam PP, Copp AJ. Cellular basis of neuroepithelial bending during mouse spinal neural tube closure. Developmental biology. 2015;404(2):113-24. doi: 10.1016/j.ydbio.2015.06.003. PubMed PMID: 26079577; PubMed Central PMCID: PMCPMC4528075.
39. Sausedo RA, Smith JL, Schoenwolf GC. Role of nonrandomly oriented cell division in shaping and bending of the neural plate. The Journal of comparative neurology. 1997;381(4):473-88. PubMed PMID: 9136804.

40. Miyata T, Okamoto M, Shinoda T, Kawaguchi A. Interkinetic nuclear migration generates and opposes ventricular-zone crowding: insight into tissue mechanics. Frontiers in cellular neuroscience. 2014;8:473. doi: 10.3389/fncel.2014.00473. PubMed PMID: 25674051; PubMed Central PMCID: PMCPMC4309187.

41. Hiscock TW, Miesfeld JB, Mosaliganti KR, Link BA, Megason SG. Feedback between tissue packing and neurogenesis in the zebrafish neural tube. Development. 2018;145(9). doi: 10.1242/dev.157040. PubMed PMID: 29678815; PubMed Central PMCID: PMCPMC5992593.

42. Kinoshita N, Sasai N, Misaki K, Yonemura S. Apical accumulation of Rho in the neural plate is important for neural plate cell shape change and neural tube formation. Molecular biology of the cell. 2008;19(5):2289-99. doi: 10.1091/mbc.E07-12-1286. PubMed PMID: 18337466; PubMed Central PMCID: PMCPMC2366863.

43. Copp AJ. Neurulation in the cranial region--normal and abnormal. Journal of anatomy. 2005;207(5):623-35. doi: 10.1111/j.1469-7580.2005.00476.x. PubMed PMID: 16313396; PubMed Central PMCID: PMCPMC1571567.

44. Schoenwolf GC, Franks MV. Quantitative analyses of changes in cell shapes during bending of the avian neural plate. Developmental biology. 1984;105(2):257-72. PubMed PMID: 6479439.

45. Smith JL, Schoenwolf GC, Quan J. Quantitative analyses of neuroepithelial cell shapes during bending of the mouse neural plate. The Journal of comparative neurology. 1994;342(1):144-51. doi: 10.1002/cne.903420113. PubMed PMID: 8207124.

46. Mitsuhashi T, Takahashi T. Genetic regulation of proliferation/differentiation characteristics of neural progenitor cells in the developing neocortex. Brain & development. 2009;31(7):553-7. doi: 10.1016/j.braindev.2009.05.002. PubMed PMID: 19464833.

47. Yamada M, Udagawa J, Hashimoto R, Matsumoto A, Hatta T, Otani H. Interkinetic nuclear migration during early development of midgut and ureteric epithelia. Anat Sci Int. 2013;88(1):31-7. doi: 10.1007/s12565-012-0156-8. PubMed PMID: 23054939.

48. Reiner O, Sapir T. LIS1 functions in normal development and disease. Current opinion in neurobiology. 2013;23(6):951-6. doi: 10.1016/j.conb.2013.08.001. PubMed PMID: 23973156.

49. Doobin DJ, Dantas TJ, Vallee RB. Microcephaly as a cell cycle disease. Cell cycle. 2017;16(3):247-8. doi: 10.1080/15384101.2016.1252591. PubMed PMID: 27792466; PubMed Central PMCID: PMCPMC5345203.

Supporting Information captions

S1 Figure. Anteroposterior growth from the forelimb to the tail bud from 2 to 4 days of development. A. Representative images of chicken embryos at stage HH13-, 18 and 23 corresponding to 48, 72 and 96 hours of incubation. The cephalic region of the embryo at stage HH18 removed prior to the picture. The green dotted line indicates the regions that was measured. B, plot of the mean length of the portion indicated in green in panel A. Dots represent the mean, error bars indicate standard deviation.

S2 Figure. Maintenance of neuroepithelial architecture requires actomyosin contractility. A, Explants of the trunk are incubated in suspension with culture medium, culture medium with DMSO or culture medium with ROCK inhibitor (Y27632, 400µM). B, Transversal sections with nuclear (DAPI, grey) and actin staining (Phalloidin, green). C, apicobasal length. D, number of pseudolayers of nuclei. E, straightness of the apical domain. F, shape of nuclei. G, position of mitoses, at scale with the tissue. H, position of mitoses, raw data (n48h=42, n72h=66, n96h=153; Kruskal-Wallis followed by multiple comparisons; ****, p<0.0001). Box and whiskers plot: the box extends from the 25th to the 75th percentile; the whiskers show the extent of the whole dataset. The median is plotted as a line inside the box.

S3 Figure. INM opposes apicobasal elongation, even with high random nuclear noise. A, Mean apicobasal (AB, open circle) and nuclear-basal (N, closed circles) lengths with normal INM (black) and low INM (red). Note that mean tissue heights goes from 75µm to 89µm in absence of INM. In the meantime, mean nuclear heights goes from 51µm to 48µm representing a shift from being located within the most apical top third of the tissue with normal INM (51µm /75µm =68%) to being located midway between the apical and basal domains

(48µm/89µm=54%). B-C, Mean width of apical (magenta), nuclear (black) and basal domain (cyan) domains with normal INM (B) or low INM conditions (C). Note that low INM conditions lead to a shrinkage of the apical domain (arrow). Error bars represent standard deviation.

S1 Table. List of parameters used in each simulations presented on Figs 3-5, 7 and S3. Yellow, passive apical-apical springs; Green, contractile apical-apical springs; blue frame, fast update of basal points; magenta, high random nuclear movement (noise); light grey, no proliferation and no INM; dark grey, low INM; bold text, normal INM conditions. The following parameters were common to all simulations: radius of nucleus soft core (Rs=5µm), radius of nucleus hard core (Rh_S=1.5µm), radius of nucleus hard core during mitosis (Rh_M=3.5µm), maximum distance between two consecutive apical points (a0=1/6*Rs), maximum distance between two consecutive basal points (b0=1/6*Rs). The relative strengths of the various forces was set as follows: stiffness of soft core of the nucleus (alpha_X=1), stiffness of apical-nucleus spring (alpha_aX=2), stiffness of nucleus-basal spring (alpha_bX=2), stiffness of apical-apical spring (alpha_aS=5), stiffness of apical-apical spring during G2 phase and mitosis (alpha_aM=10), magnitude of the apical-nucleus-basal alignment force (alpha_ab=15).

S1 Movie (related to Figure 2). Mosaic expression of membrane-GFP (green) and membrane-mCherry (red) into the chick neuroepithelium at stage HH14 at the level of the intermediate neural tube. Nuclei are counterstained with DAPI (grey).

S2 Movie (related to Figures 3 and 4). All simulations start with 30 cells. Exclusion rate of daughter cells is set to 50% keeping the total cell number constant. Top panels: simulations with passive apical-apical springs without INM (left), with low INM (middle), with normal INM (right). Bottom panels: simulations with contractile apical-apical springs without INM (left), with low INM (middle), with normal INM (right). Note that in absence of INM there is a rapid shrinkage of the apical domain giving the tissue a pyramidal shape. Also, INM leads the rapid emergence of a low nuclear density region basally. Only hard cores of nuclei, apical points and basal points are represented. Soft cores of nuclei and springs are not displayed. Red, cells in mitosis; yellow cells in PRAM/active G2; black line, tracking of nuclei in PRAM/G2 and M. Each frame corresponds to one iteration of the simulation (circa. 6 minutes of biological time). Total duration 480 iterations (48h of biological time).

S3 Movie (related to Figure 5). All simulations start with 30 cells with normal INM. From left to right, exclusion rate of daughter cells is set to 50% (constant cell number), 40%, 30%, 0% (all daughter cells added to the 2D plane). Top panels: simulations with passive apical-apical springs. Bottom panels: simulations with contractile apical-apical springs. Note that contractile apical springs mitigates buckling of the apical domain and feeds back into basal rearrangements. Red, cells in mitosis; yellow cells in PRAM/active G2; black line, tracking of nuclei in PRAM/G2 and M. Each frame corresponds to one iteration of the simulation (circa. 6 minutes of biological time). Total duration 480 iterations (48h of biological time).

S4 Movie (related to figure 7). All simulations start with 30 cells with normal INM and a 25-fold increase of random nuclear displacement at each iteration (noise) compared to previous simulations. From left to right, exclusion rate of daughter cells is set to 50% (constant cell number), 40% and 30%. The fourth condition at the far-right is with 30% of exclusion rate and fast update of basal points. Note that the global non-oriented force generated by increased noise is converted into apicobasal elongation. Also, allowing fast reorganization of the basal points promotes isotropic expansion of the apical and basal domain. Red, cells in mitosis; yellow, cells in PRAM/active G2; black line, tracking of nuclei in PRAM/G2 and M. Each frame corresponds to one iteration of the simulation (circa. 6 minutes of biological time). Total duration 480 iterations (48h of biological time).

S5 Movie (related to Supplementary Figure 3). Simulations start with 30 cells. Exclusion rate is set to 50% (constant cell number). Left panel, normal INM. Right panel, low INM conditions. Note that without normal INM the apicobasal expansion is faster and that there is a shrinkage of the apical domain.

Supplementary Information. This file contains the details about the mathematical model.

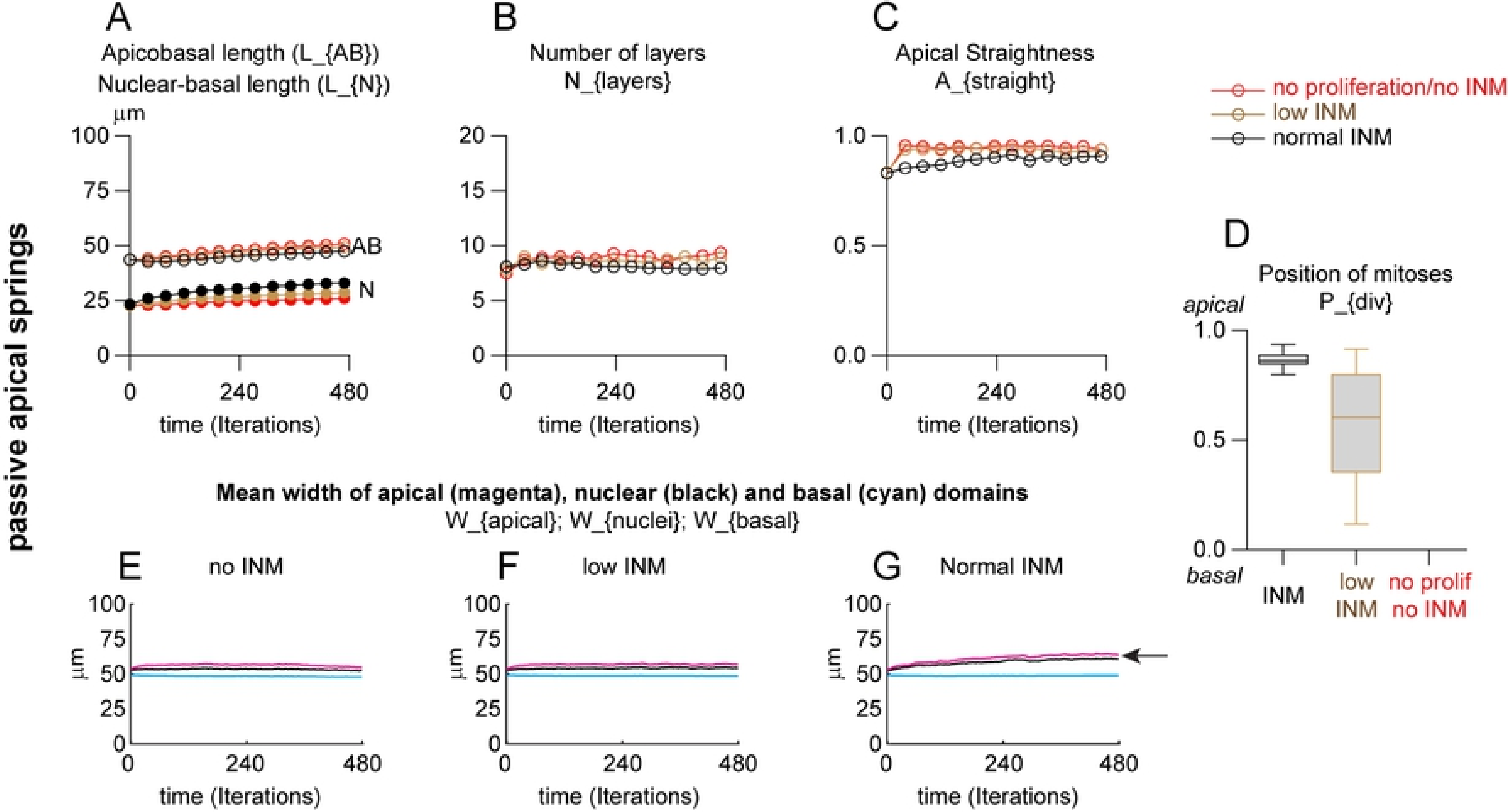
passive apical springs
A
Apicobasal length (L_{AB})
Nuclear-basal length (L_{N})
µm
100
75
50
25
0
AB
N
0
240
480
time (Iterations)
B
Number of layers
N_{layers}
20
15
10
5
0
C
Apical Straightness
A_{straight}
1.0
0.5
0.0
no proliferation/no INM
low INM
normal INM
D
Position of mitoses
P_{div}
apical
basal
INM
low INM
no prolif no INM
Mean width of apical (magenta), nuclear (black) and basal (cyan) domains
W_{apical}; W_{nuclei}; W_{basal}
E
no INM
F
low INM
G
Normal INM
µm

Figure 3

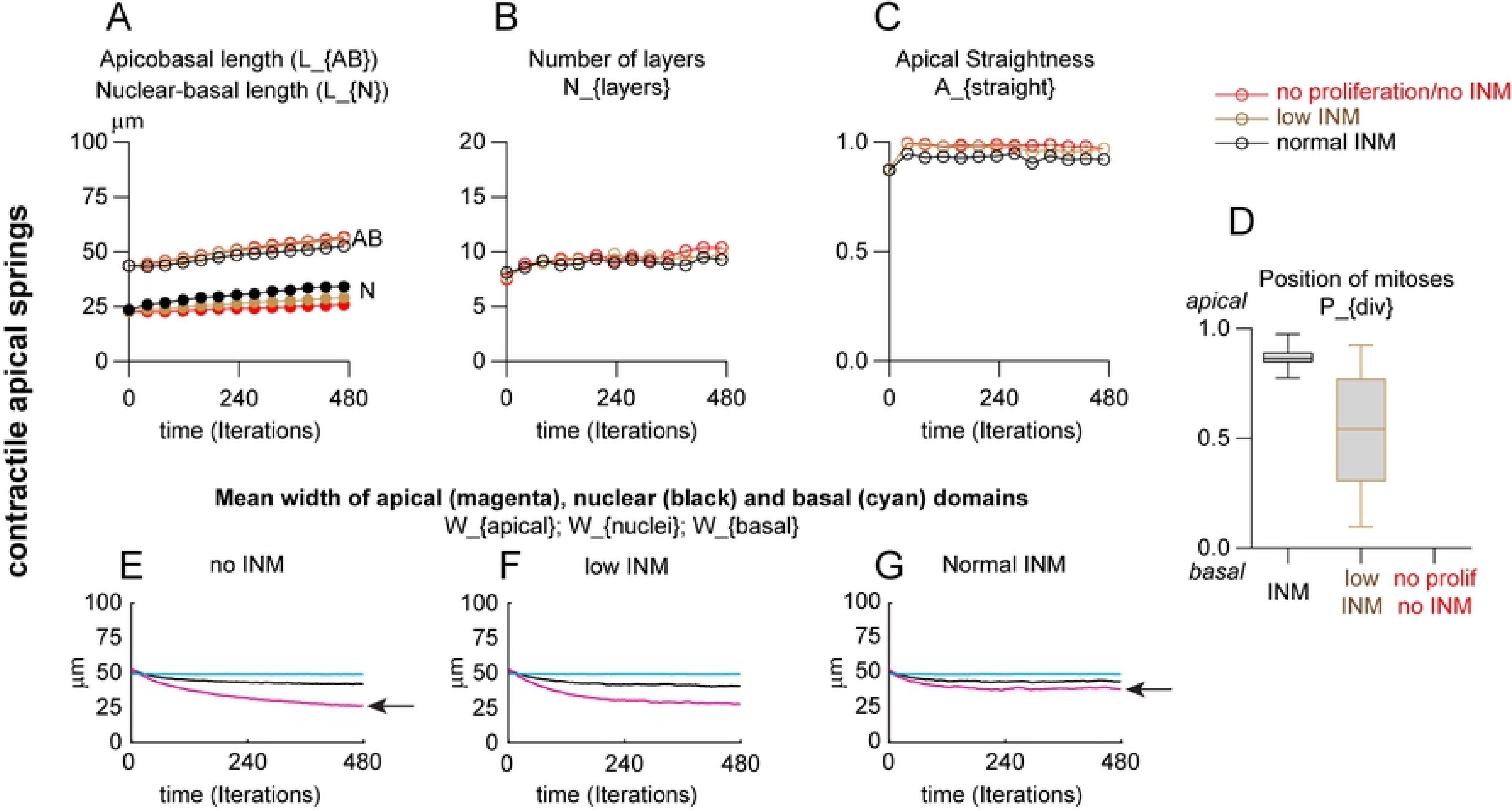
contractile apical springs
A
Apicobasal length (L_{AB})
Nuclear-basal length (L_{N})
μm
100
75
50
25
0
AB
N
0
240
480
time (Iterations)
B
Number of layers
N_{layers}
20
15
10
5
0
0
240
480
time (Iterations)
C
Apical Straightness
A_{straight}
1.0
0.5
0.0
0
240
480
time (Iterations)
no proliferation/no INM
low INM
normal INM
D
Position of mitoses
P_{div}
apical
basal
1.0
0.5
0.0
INM
low INM
no prolif no INM
Mean width of apical (magenta), nuclear (black) and basal (cyan) domains
W_{apical}; W_{nuclei}; W_{basal}
E
no INM
F
low INM
G
Normal INM
100
75
50
25
0
μm
0
240
480
time (Iterations)

Figure 4

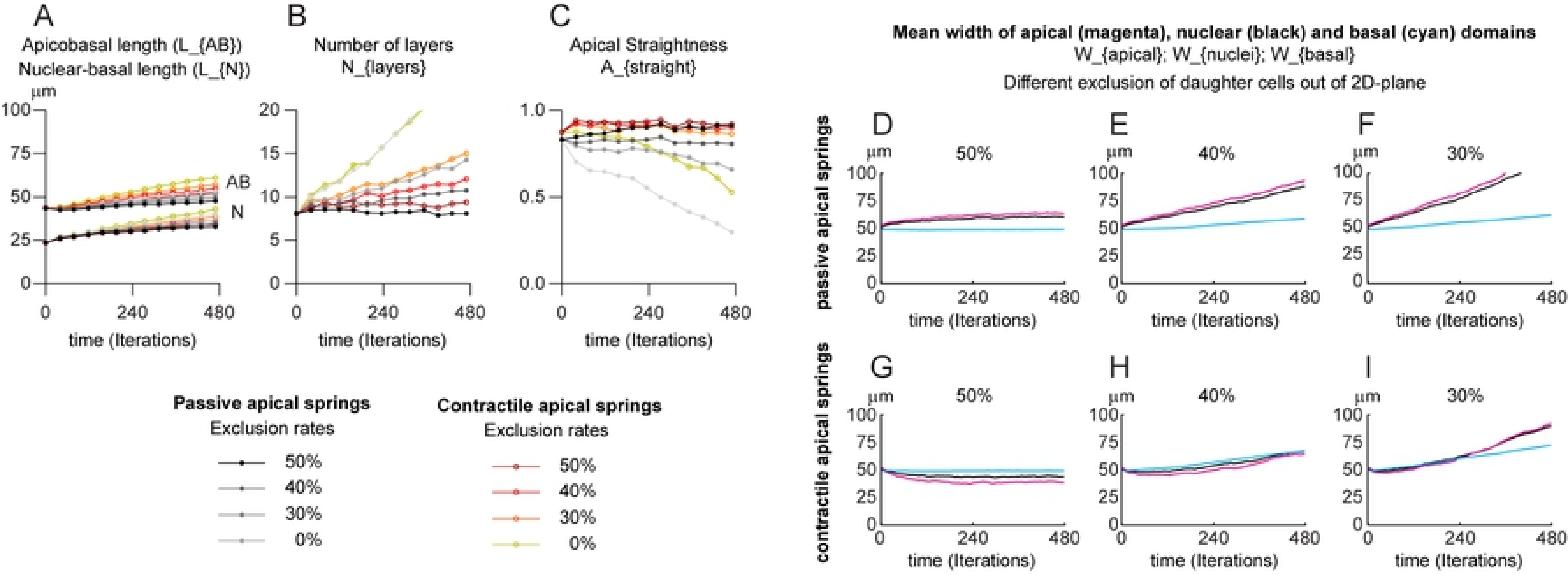
A
Apicobasal length (L_{AB})
Nuclear-basal length (L_{N})
µm
100
75
50
25
0
AB
N
0
240
480
time (Iterations)
B
Number of layers
N_{layers}
20
15
10
5
0
0
240
480
time (Iterations)
C
Apical Straightness
A_{straight}
1.0
0.5
0.0
0
240
480
time (Iterations)
Mean width of apical (magenta), nuclear (black) and basal (cyan) domains
W_{apical}; W_{nuclei}; W_{basal}
Different exclusion of daughter cells out of 2D-plane
passive apical springs
D
µm
50%
E
µm
40%
F
µm
30%
100
75
50
25
0
0
240
480
time (Iterations)
contractile apical springs
G
µm
50%
H
µm
40%
I
µm
30%
100
75
50
25
0
0
240
480
time (Iterations)
Passive apical springs
Exclusion rates
50%
40%
30%
0%
Contractile apical springs
Exclusion rates
50%
40%
30%
0%

Figure 5

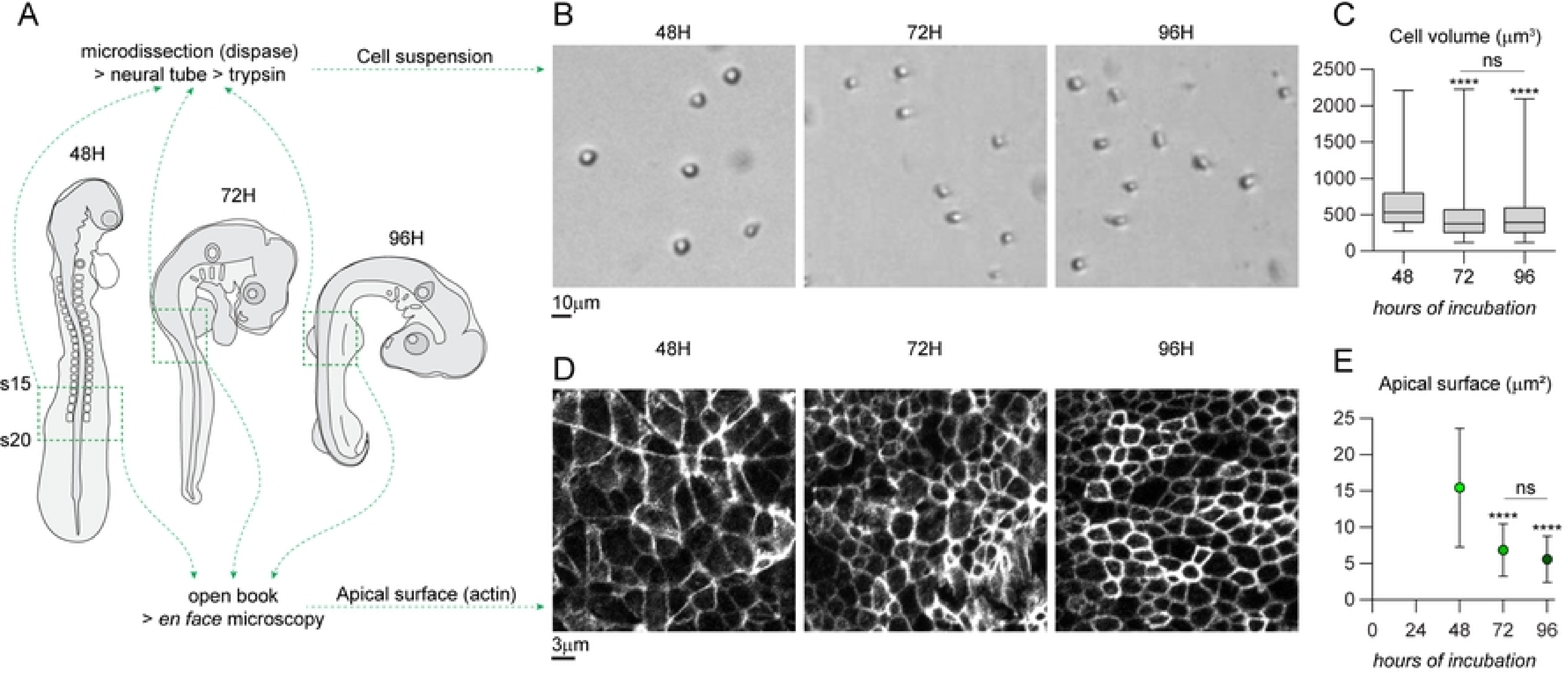
A
microdissection (dispase)
> neural tube > trypsin
Cell suspension
48H
72H
96H
s15
s20
open book
> en face microscopy
Apical surface (actin)
B
48H
72H
96H
10μm
C
Cell volume (μm³)
ns
****
****
2500
2000
1500
1000
500
0
48
72
96
hours of incubation
D
48H
72H
96H
3μm
E
Apical surface (μm²)
ns
****
****
25
20
15
10
5
0
0
24
48
72
96
hours of incubation

Figure 6

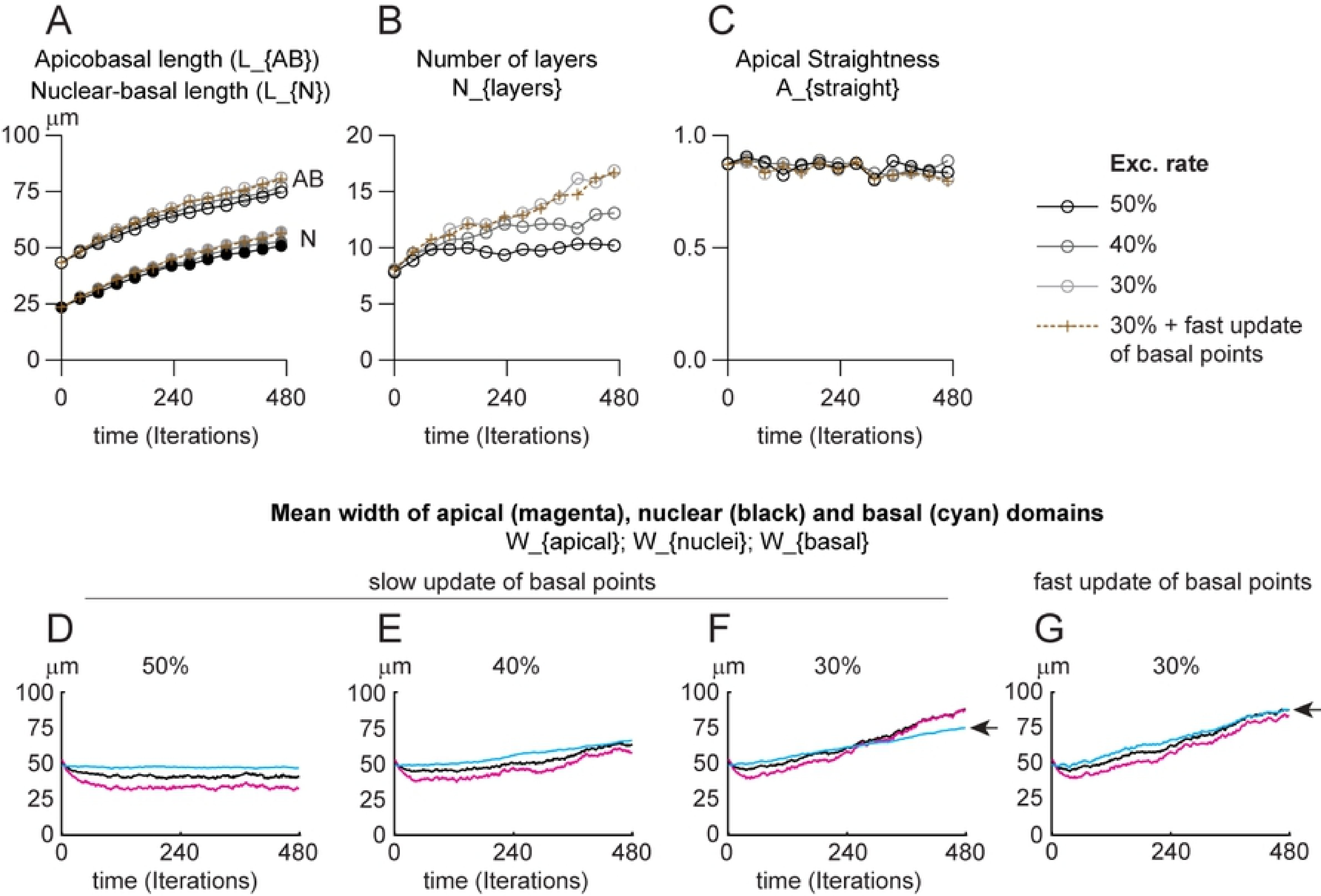
A
Apicobasal length (L_{AB})
Nuclear-basal length (L_{N})
µm
100
75
50
25
0
AB
N
0
240
480
time (Iterations)
B
Number of layers
N_{layers}
20
15
10
5
0
0
240
480
time (Iterations)
C
Apical Straightness
A_{straight}
1.0
0.5
0.0
0
240
480
time (Iterations)
Exc. rate
50%
40%
30%
30% + fast update of basal points
Mean width of apical (magenta), nuclear (black) and basal (cyan) domains
W_{apical}; W_{nuclei}; W_{basal}
slow update of basal points
fast update of basal points
D
µm
50%
100
75
50
25
0
0
240
480
time (Iterations)
E
µm
40%
100
75
50
25
0
0
240
480
time (Iterations)
F
µm
30%
100
75
50
25
0
0
240
480
time (Iterations)
G
µm
30%
100
75
50
25
0
0
240
480

Figure 7

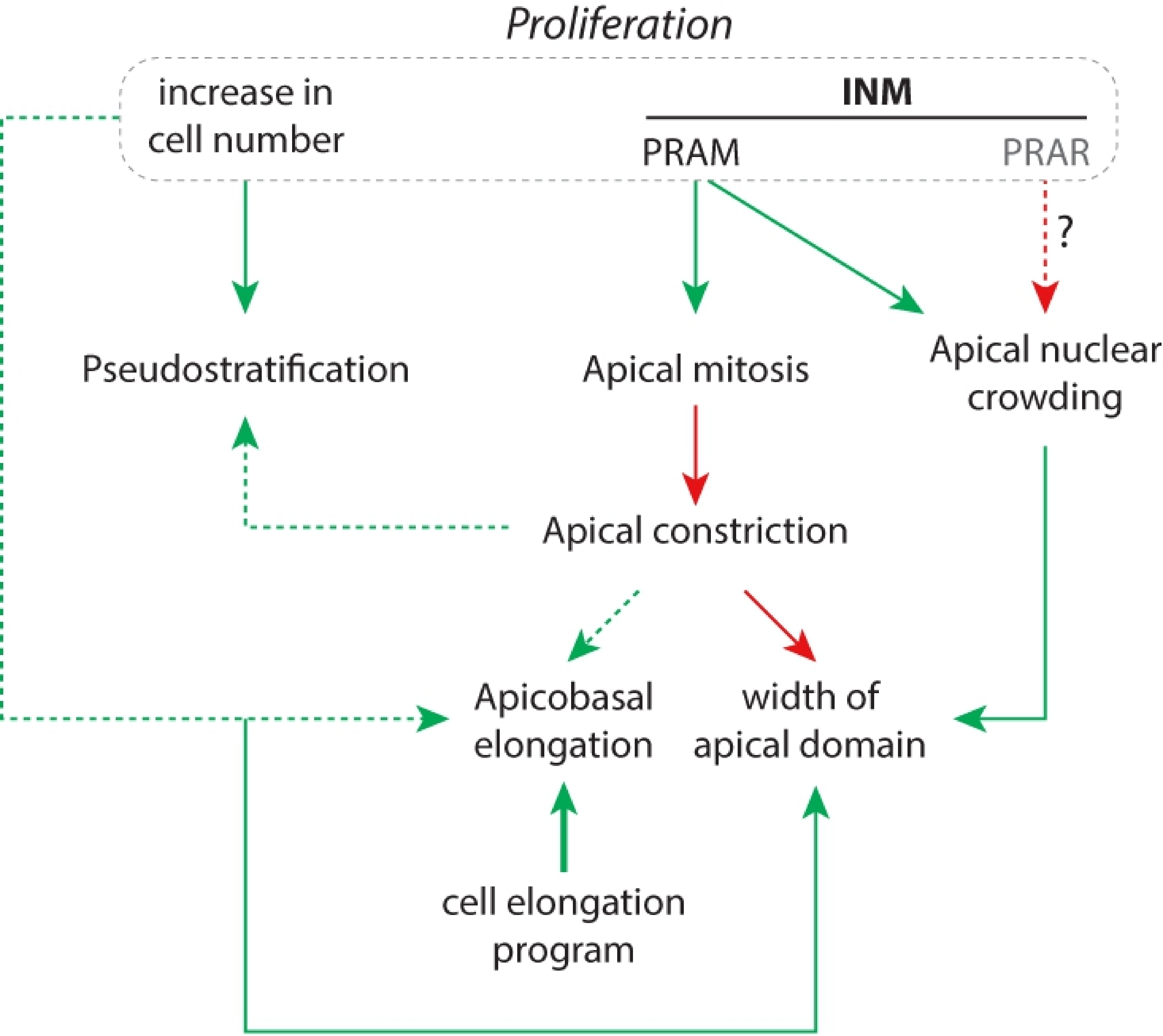
Proliferation
increase in cell number
INM
PRAM
PRAR
?
Pseudostratification
Apical mitosis
Apical nuclear crowding
Apical constriction
Apicobasal elongation
width of apical domain
cell elongation program

Figure 8

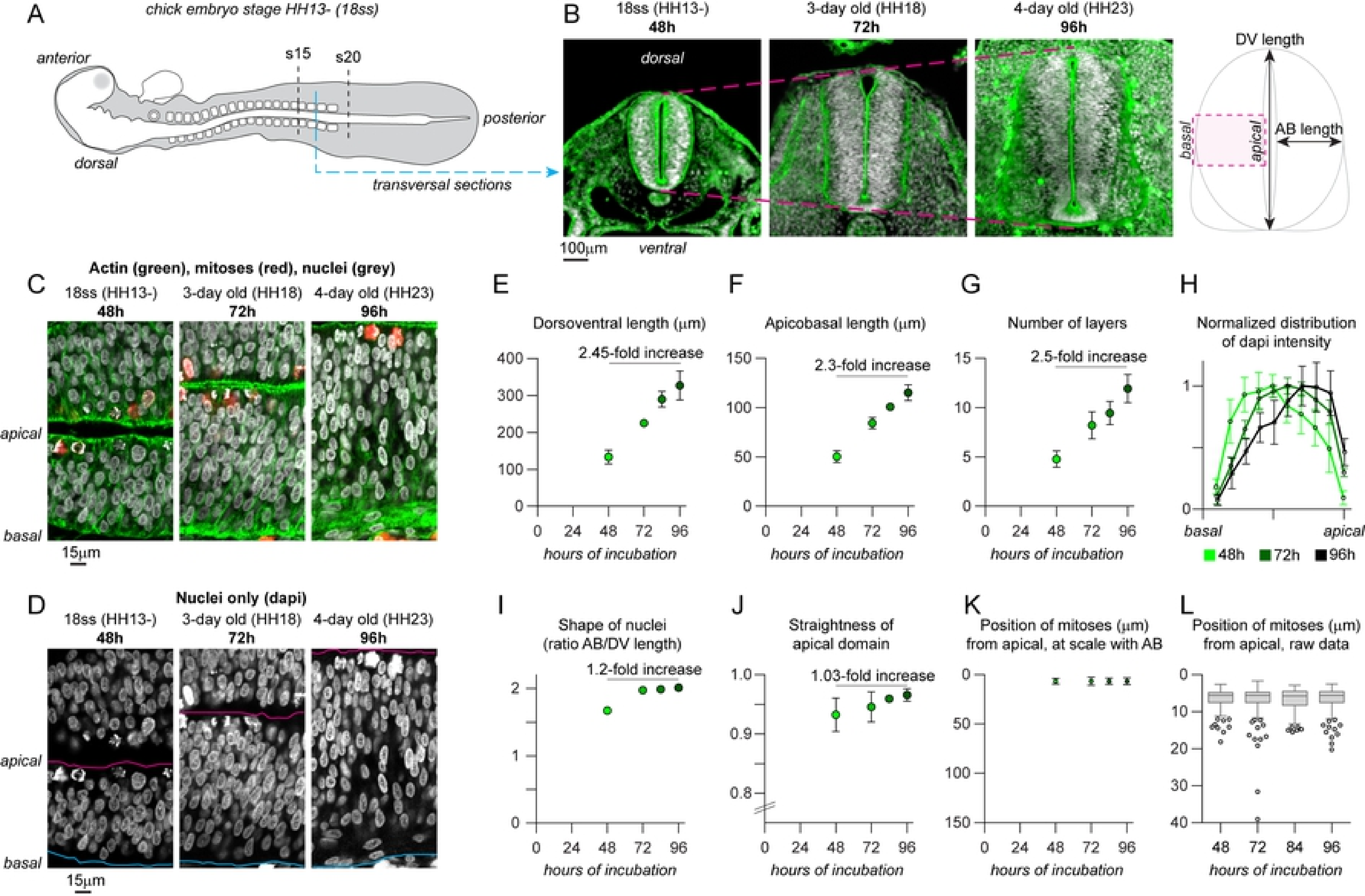
A
chick embryo stage HH13- (18ss)
anterior
s15
s20
posterior
dorsal
transversal sections
B
18ss (HH13-)
48h
3-day old (HH18)
72h
4-day old (HH23)
96h
dorsal
ventral
100μm
DV length
AB length
basal
apical
C
Actin (green), mitoses (red), nuclei (grey)
18ss (HH13-)
48h
3-day old (HH18)
72h
4-day old (HH23)
96h
apical
basal
15μm
D
Nuclei only (dapi)
18ss (HH13-)
48h
3-day old (HH18)
72h
4-day old (HH23)
96h
apical
basal
15μm
E
Dorsoventral length (μm)
2.45-fold increase
400
300
200
100
0
0 24 48 72 96
hours of incubation
F
Apicobasal length (μm)
2.3-fold increase
150
100
50
0
0 24 48 72 96
hours of incubation
G
Number of layers
2.5-fold increase
15
10
5
0
0 24 48 72 96
hours of incubation
H
Normalized distribution of dapi intensity
1
0
basal
apical
48h
72h
96h
I
Shape of nuclei (ratio AB/DV length)
1.2-fold increase
2
1
0
0 24 48 72 96
hours of incubation
J
Straightness of apical domain
1.03-fold increase
1.0
0.9
0.8
0 24 48 72 96
hours of incubation
K
Position of mitoses (μm) from apical, at scale with AB
0
50
100
150
0 24 48 72 96
hours of incubation
L
Position of mitoses (μm) from apical, raw data
0
10
20
30
40
48 72 84 96
hours of incubation

Figure 1

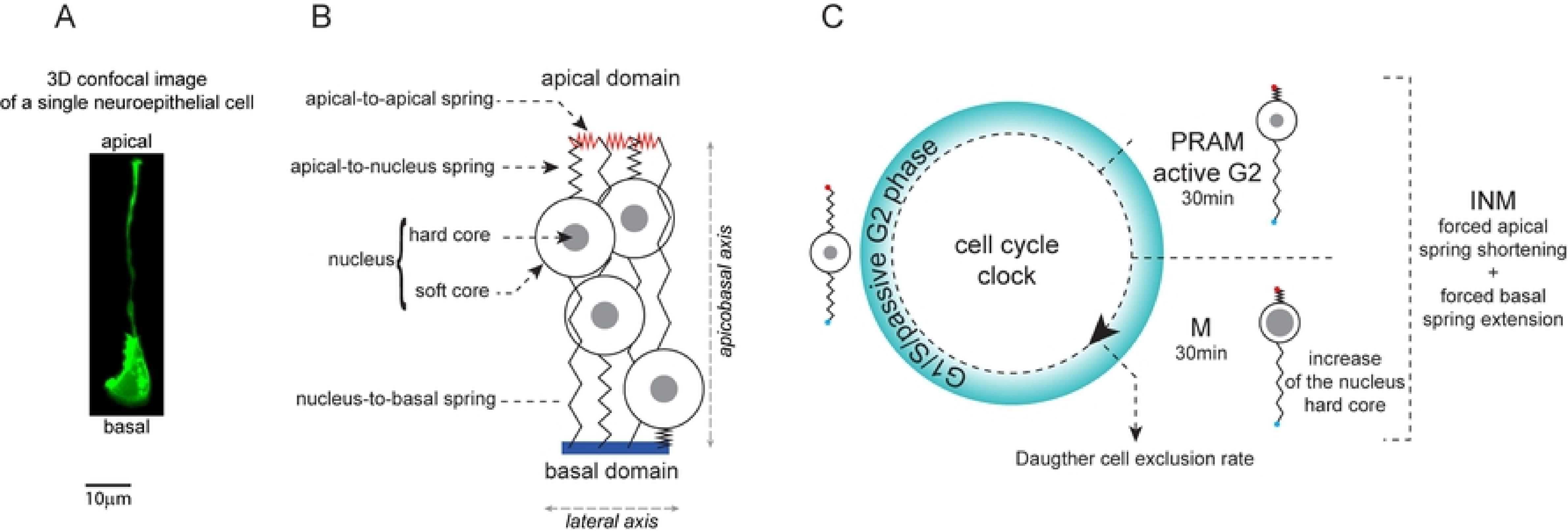
A
3D confocal image
of a single neuroepithelial cell
apical
basal
10µm
B
apical domain
apical-to-apical spring
apical-to-nucleus spring
nucleus
hard core
soft core
nucleus-to-basal spring
basal domain
apicobasal axis
lateral axis
C
G1/S/passive G2 phase
cell cycle
clock
PRAM
active G2
30min
M
30min
Daugther cell exclusion rate
increase
of the nucleus
hard core
INM
forced apical
spring shortening
+
forced basal
spring extension

Figure 2

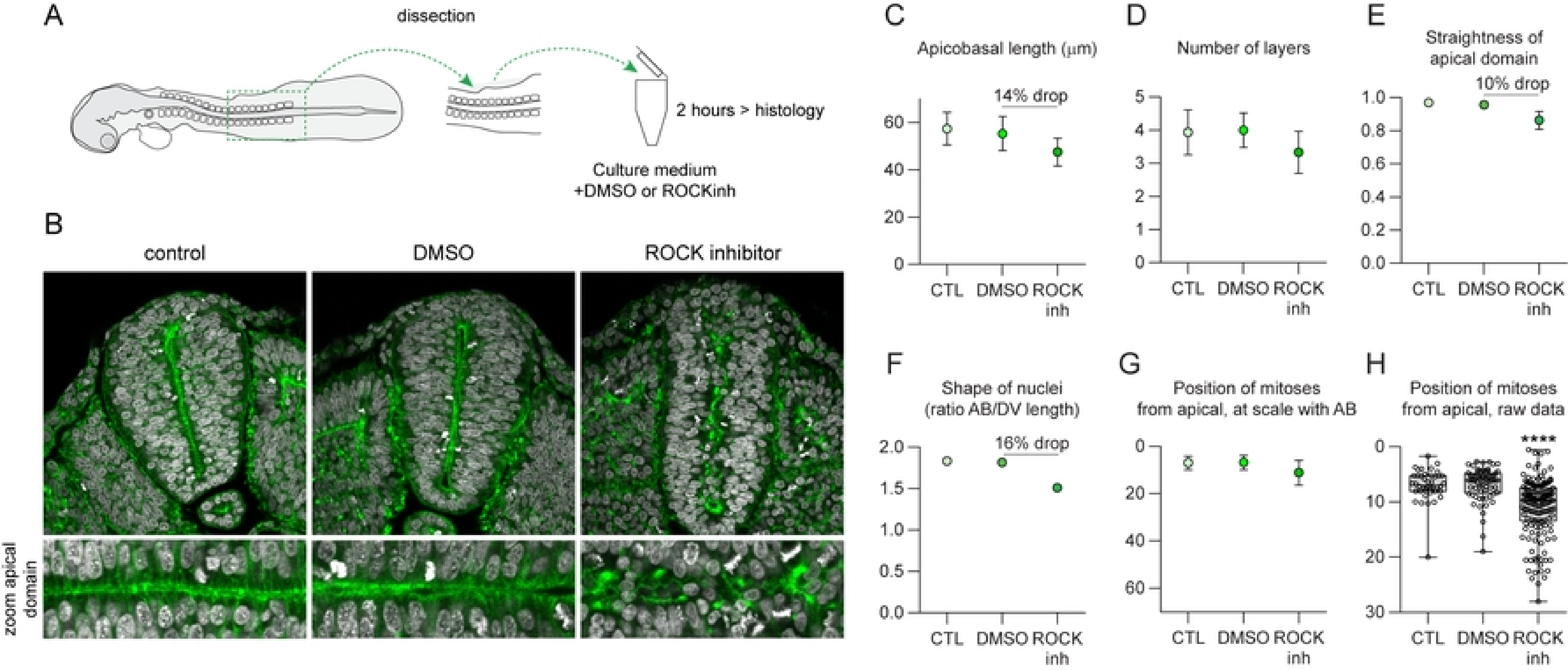
A
dissection
2 hours > histology
Culture medium
+DMSO or ROCKinh
B
control
DMSO
ROCK inhibitor
zoom apical domain
C
Apicobasal length (μm)
14% drop
0
20
40
60
CTL
DMSO
ROCK inh
D
Number of layers
0
1
2
3
4
5
CTL
DMSO
ROCK inh
E
Straightness of apical domain
10% drop
0.0
0.2
0.4
0.6
0.8
1.0
CTL
DMSO
ROCK inh
F
Shape of nuclei (ratio AB/DV length)
16% drop
0.0
0.5
1.0
1.5
2.0
CTL
DMSO
ROCK inh
G
Position of mitoses from apical, at scale with AB
0
20
40
60
CTL
DMSO
ROCK inh
H
Position of mitoses from apical, raw data
****
0
10
20
30
CTL
DMSO
ROCK inh

Figure S2

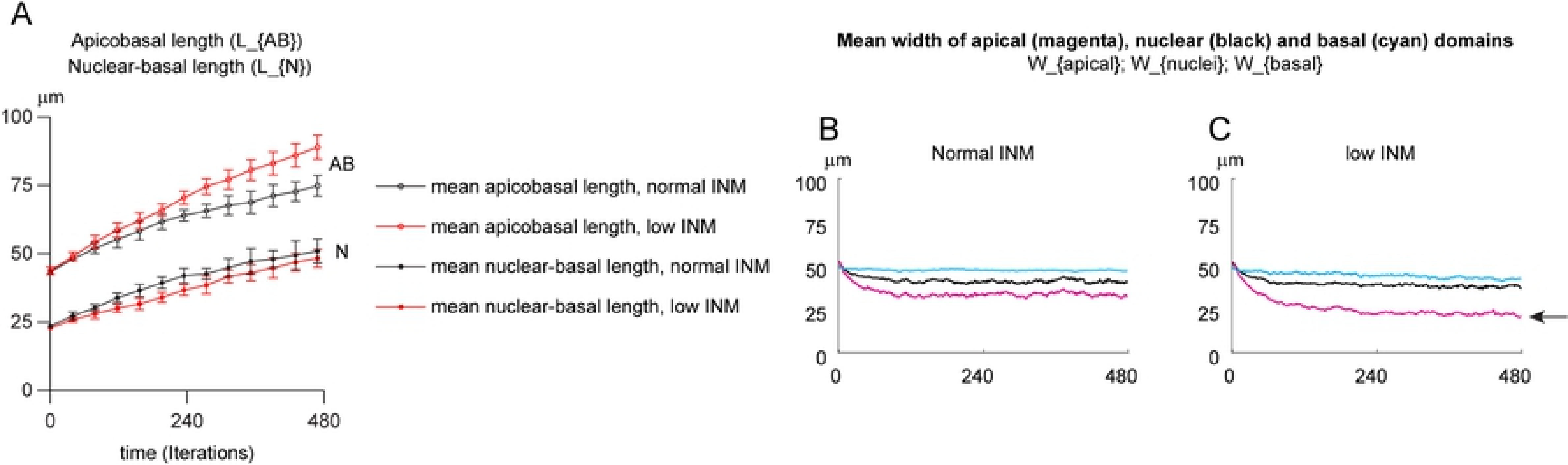
A
Apicobasal length (L_{AB})
Nuclear-basal length (L_{N})
µm
100
75
50
25
0
0
240
480
time (Iterations)
AB
N
mean apicobasal length, normal INM
mean apicobasal length, low INM
mean nuclear-basal length, normal INM
mean nuclear-basal length, low INM
Mean width of apical (magenta), nuclear (black) and basal (cyan) domains
W_{apical}; W_{nuclei}; W_{basal}
B
Normal INM
µm
100
75
50
25
0
0
240
480
C
low INM
µm
100
75
50
25
0
0
240
480

Figure S3

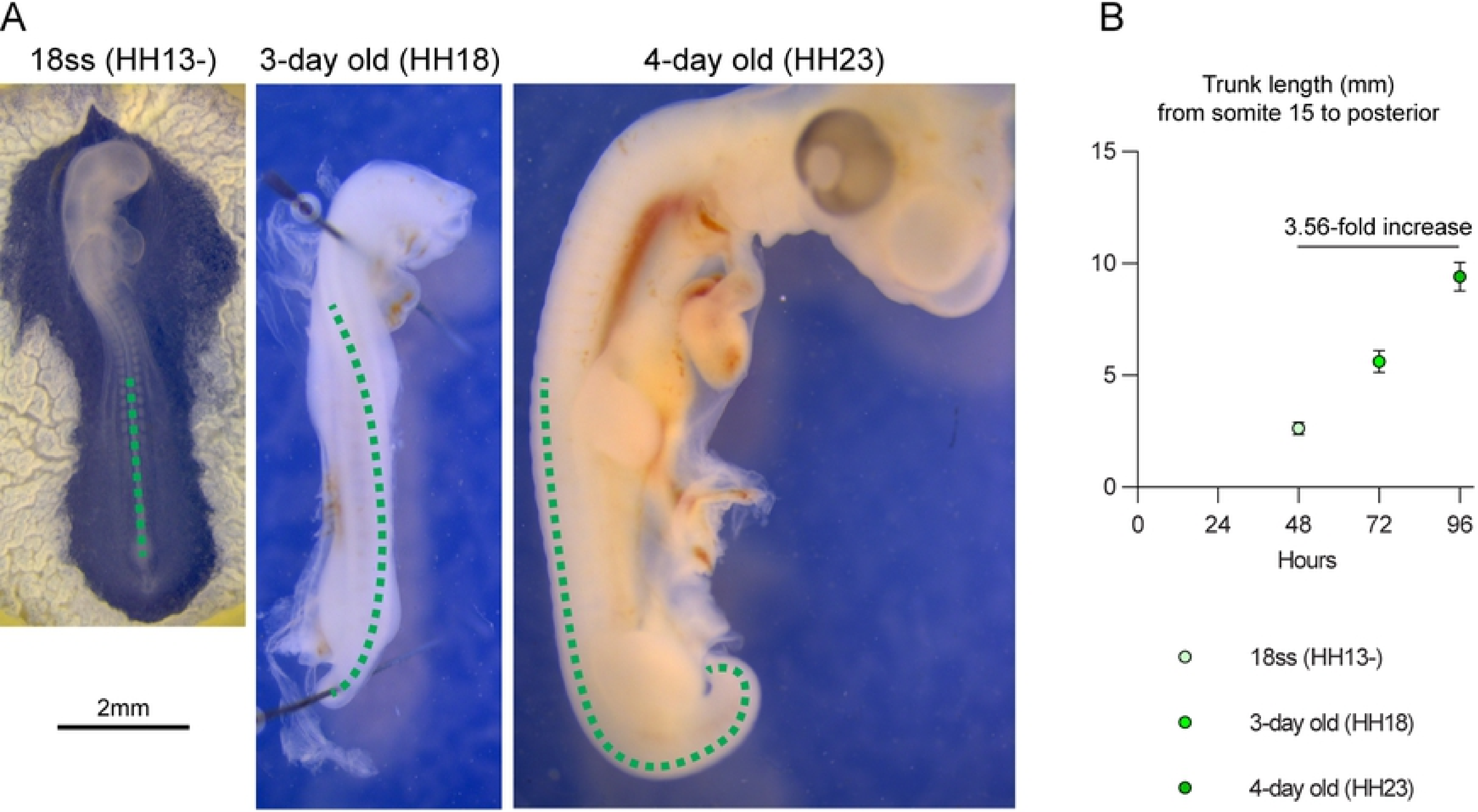
A
18ss (HH13-)
3-day old (HH18)
4-day old (HH23)
2mm
B
Trunk length (mm)
from somite 15 to posterior
15
10
5
0
3.56-fold increase
0
24
48
72
96
Hours
○ 18ss (HH13-)
● 3-day old (HH18)
● 4-day old (HH23)

Figure S1